analysis revealed that enrichment of H3K9me3 was markedly reduced compared with that at the *Gapdh* promoter region in the four-cell stage (5′-R, 0.83-fold upregulated; XP, 2.85-fold upregulated; RA, 4.8-fold upregulated; Fig. 4e). These results suggested that demethylation at the promoter region was essential for Xm-*Xist* derepression.

We then asked whether *Xist* promoter demethylation was involved in the Xm-*Xist* derepression observed in *Kdm4b*-PEs at the four-cell stage. The H3K9me3 levels at major satellite regions in *Kdm4b*-PEs were significantly reduced compared with those in *Egfp*-PEs (*Kdm4b*-PEs: 9.74% versus *Egfp*-PEs: 24.63%, $P<0.01$, Student's *t*-tests; Fig. 4f). At three *Xist* regions, the H3K9me3

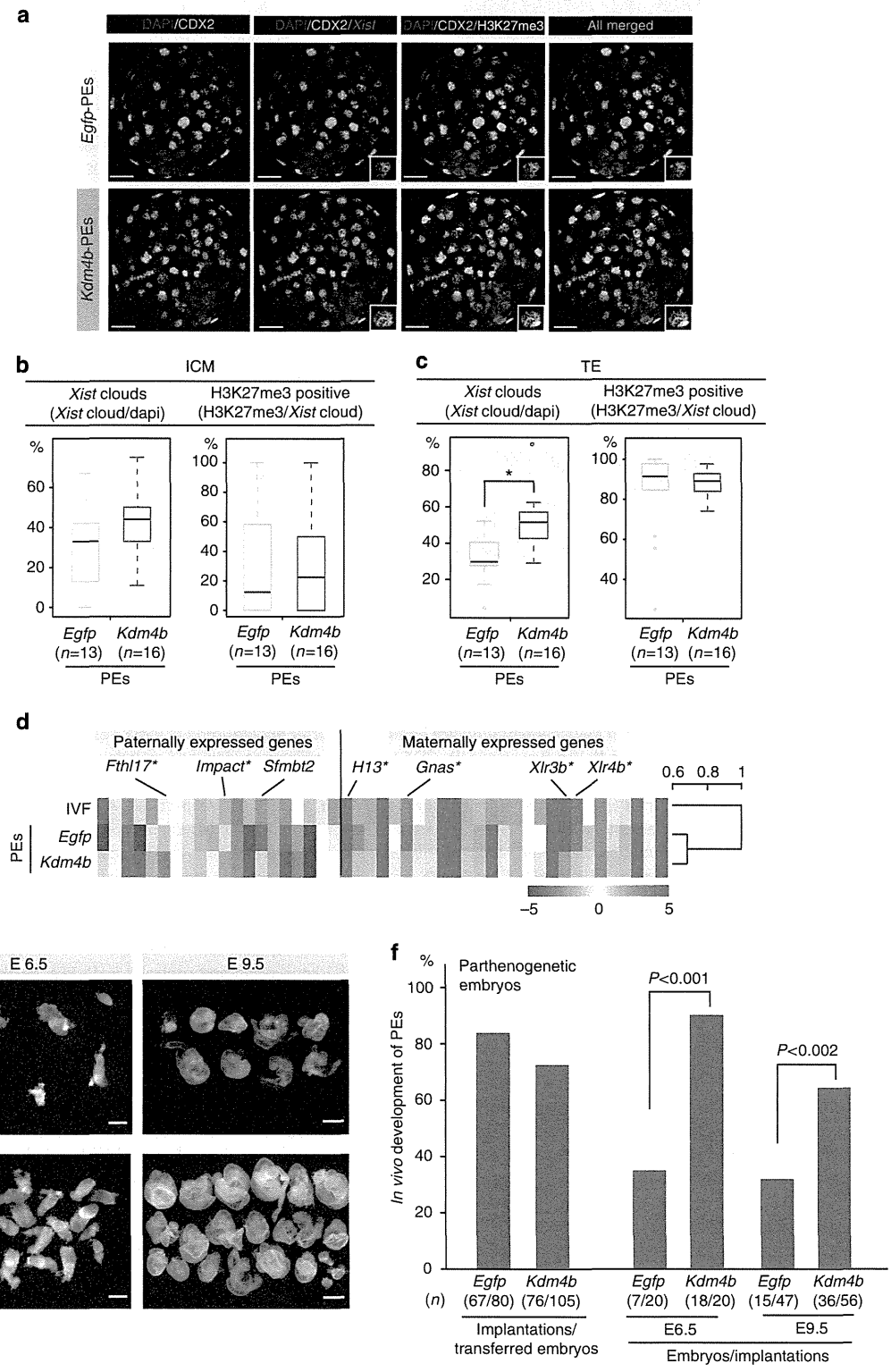

Figure 5

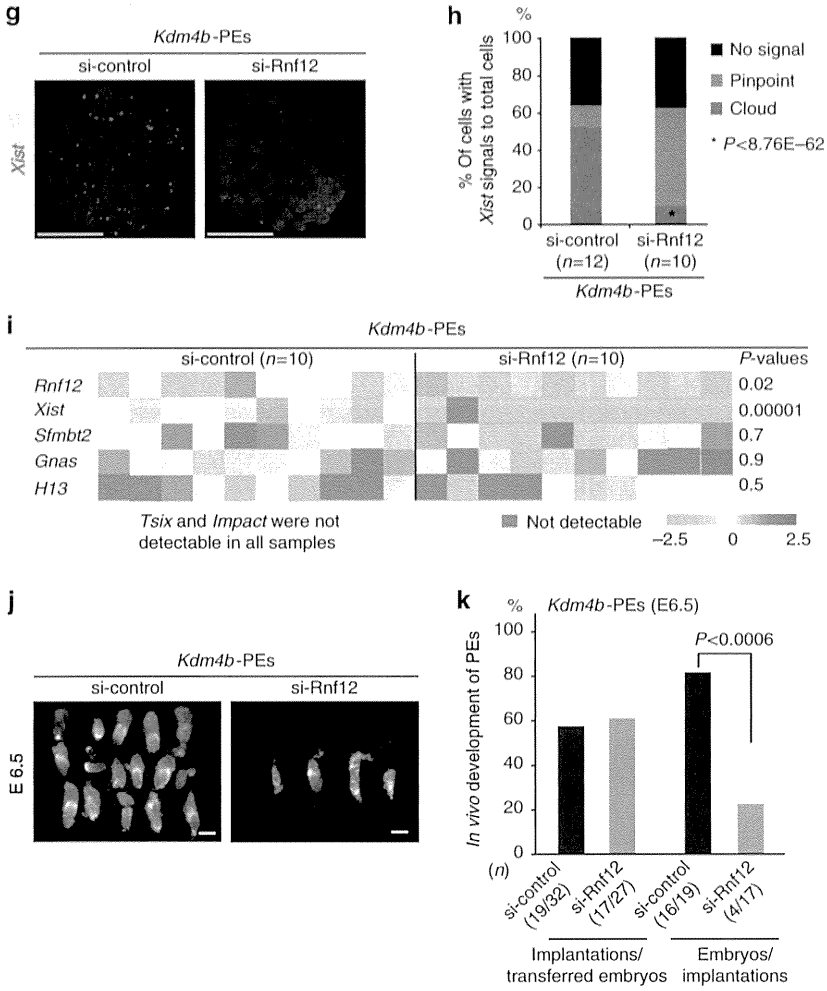

Figure 5 | Loss of Xm-XCI is the primary cause of developmental failure immediately after implantation in most PEs. (**a**) IF combined with FISH analysis of blastocysts in *Egfp*-PEs (upper panel) and *Kdm4b*-PEs (lower panel). CDX2-positive cells were identified as belonging to the trophectoderm (TE). Representative pictures of Z-sections. 4′,6-diamidino-2-phenylindole (DAPI) (blue), CDX2 (green), *Xist* (red) and H3K27me3 (white). Scale bars, 20 μm. The rates of cells with *Xist* (left) or H3K27me3 (right) in the inner cell mass (ICM) (**b**) and TE (**c**), respectively. *n*, number of embryos analysed. The number of cells analysed is shown in Supplementary Table 7. $^{*}P<4.3\times10^{-23}$ (Fisher's exact test). (**d**) Expression states and clustering analysis of imprinted genes. *Sfmbt2* important for placentation and differentially expressed genes (asterisk) are shown. The scale bar indicates normalized values of $\log_2$. (**e**) Embryos with extra-embryonic tissues at E6.5 and E9.5 for *Kdm4b*- and *Egfp*-PEs, respectively. Upper and lower images indicate *Egfp*- and *Kdm4b*-PEs, respectively. Left and right column sides show E6.5 and E9.5, respectively. Scale bars, 200 μm (E6.5) and 500 μm (E9.5). (**f**) Summary of the developmental abilities of *Kdm4b*-PEs and *Egfp*-PEs at postimplantation stages (E6.5 and E9.5). Five and 12 independent recipients were analysed at E6.5 and E9.5, respectively. (**g**,**h**) *Xist* analysis in *Rnf12*-knockdown and control *Kdm4b*-PEs. Representative images of FISH analysis. Scale bars, 50 μm (**g**) and *Xist* expression states (**h**). (**i**) Expression of imprinted and X-linked genes in *Rnf12*-knockdown and control *Kdm4b*-PEs. *P*-values were determined using Student's *t*-tests. (**j**) Embryos with extra-embryonic tissues at E6.5 in *Rnf12*-knockdown and control *Kdm4b*-PEs. Scale bars, 200 μm. (**k**) Summary of the developmental ability of *Rnf12*-knockdown and control *Kdm4b*-PEs at E6.5. Five independent recipients were analysed. The *P*-values were determined using Fisher's exact test.

levels of the promoter region in *Kdm4b*-PEs were significantly reduced, as follows: 5′-R, *Kdm4b*-PEs: 0.84% versus *Egfp*-PEs: 11.48%, $P<0.05$, Student's *t*-tests; XP, *Kdm4b*-PEs: 3.13% versus *Egfp*-PEs: 16.08%; $P<0.04$, Student's *t*-tests; and RA, *Kdm4b*-PEs: 20.16% versus *Egfp*-PEs: 29.99%; Fig. 4g. Taken together, these results demonstrated that H3K9me3 at the promoter region protected Xm-*Xist*, preventing RNF12-mediated activation from the four-cell stage. We concluded that silencing of Xm-*Xist* by imprinting to establish iXCI involved H3K9me3.

Maternal repressive H3K9me3 mark is absent in ES cells. Previous studies have shown that *Xist* is ectopically expressed in embryos cloned from somatic and ES cells[27,28]. However, the cause of aberrant *Xist* expression in cloned embryos remains unknown. Given that high H3K9me3 levels at the promoter region in PEs are lost during development (Fig. 4d,e), we investigated whether the maternal repressive H3K9me3 mark was lost in ES cells and whether *Xist* in ES cells was permissive against RNF12 during oocyte-mediated reprogramming.

To test this possibility, we first examined H3K9me3 states at *Xist* regions in various types of male ES cells, using published data[29,30]. The levels of H3K9me3 at *Xist* regions containing promoters in TT2 and E14 ES cell lines were low compared with those in positive control regions (Supplementary Fig. 9). ChIP-seq analysis revealed that although ectopic expression of KDM4B

in male ES cells induced global H3K9me3 demethylation (Supplementary Fig. 10a–d), it did not alter H3K9me3 levels at *Xist* regions. Moreover, these levels were low compared with those of a known H3K9me3-rich region (Supplementary Fig. 10e)[16]. Furthermore, the expression of *Xist* in cloned embryos was also not affected by ectopic expression of KDM4B (Supplementary Fig. 10f). These results indicated that the maternal repressive H3K9me3 mark was lost.

To establish whether RNF12 is involved in *Xist* activation during oocyte-mediated reprogramming, oocytes treated with si-*Rnf12* were used as recipients for nuclear transfer (Supplementary Fig. 10g). At the four-cell stage, derepression of *Xist* transcription in ES-cloned embryos depended on RNF12 (>50% repression in si-*Rnf12* group; Supplementary Fig. 10h). Taken together, these data indicated that the intrinsic H3K9me3 mark, which was essential for repression of *Xist* by RNF12, was lost during embryo development. This indicated that the primary cause of aberrant *Xist* expression in cloned embryos was involved in loss of intrinsic H3K9me3 at *Xist* regions.

Effects of iXCI disruption on FEs. The effects of Xm-*Xist* derepression on postimplantation development remain unclear. First, we asked whether ectopic *Kdm4b* expression caused Xm-*Xist* derepression in FEs. *Kdm4b*-FEs developed into blastocysts with high efficiency (>80% of two-cell embryos; Supplementary Table 6). At the 96-h blastocyst stage, *Xist* transcription was derepressed in male *Kdm4b*-FEs, while *Pgk1* and *Plac1* levels were reduced to <13% of those observed in controls (Supplementary Fig. 11a). In female *Kdm4b*-FEs, FISH analysis revealed that there were cells with *Xist* biallelic expression (Supplementary Fig. 11b). Although the expression level was slightly elevated (1.3-fold), X-linked genes were also significantly repressed in female *Kdm4b*-FEs (Supplementary Fig. 11c). These results showed that ectopic Xm-*Xist* derepression caused X-linked gene silencing and elimination of iXCI.

To test the effects of iXCI disruption on postimplantation development, we conducted *in vivo* transplantation experiments. Interestingly, our results demonstrated that XCI on Xm during preimplantation did not affect developmental competence to term (*Kdm4b*-FEs: 63.2% versus *Egfp*-FEs: 53.1%; Supplementary Fig. 11d,e), suggesting that aberrant XCI in preimplantation embryos was restored during postimplantation development, probably through an automatic counting function. These results were consistent with the observation that the developmental competency of embryonic cloned embryos was high, despite the ectopic expression of *Xist* and the occurrence of global XCI (Supplementary Fig. 12)[28,31].

Loss of XCI impairs the postimplantation development of PEs. It is still unknown whether the embryonic lethality observed immediately after implantation in the majority of PEs (around 70–80%) can be attributed to the loss of dysregulation of X-linked genes or to loss of expression of autosomal paternally imprinted genes. Figure 2 showed that the percentage of *Xist*-positive cells in *Kdm4b*-PEs was significantly higher than that in *Egfp*-PEs. Thus, we reasoned that *Kdm4b*-PEs would be suitable for studying this long-standing question.

We first performed a detailed analysis of Xm-XCI states in *Kdm4b*-PEs using IF against H3K27me3 and CDX2, a marker of the trophectoderm, in combination with *Xist* FISH, at the blastocyst stage. This analysis revealed that *Xist*-positive cells were significantly increased in the trophectoderm of *Kdm4b*-PEs, although the ratio of H3K27me3-positive cells was comparable to that of *Egfp*-PEs (Fig. 5a–c and Supplementary Table 7). However, no significant difference was observed in the inner cell mass between groups (Fig. 5a–c and Supplementary Table 7), indicating that loss of H3K9me3 in the maternal genome led to establishment of Xm-XCI as an imprinted Xp-XCI.

Next, we carried out transcriptome analysis in *Egfp*-PEs, *Kdm4b*-PEs and FEs using microarray. Clustering analysis based on gene expression patterns showed that all three groups could be distinguished clearly from each other (Supplementary Fig. 13a). Comparison of transcripts between *Egfp*-PEs and *Kdm4b*-PEs identified transcripts that were significantly differentially expressed: 671 transcripts were upregulated and 711 transcripts were downregulated ($P<0.05$, Student's *t*-test and >1.5-fold changes in *Kdm4b*-PEs). Chromosome distribution analysis showed that upregulated transcripts in *Kdm4b*-PEs were distributed across various chromosomes (2.33–7.23%; Supplementary Fig. 13b). However, downregulated transcripts in *Kdm4b*-PEs were mostly concentrated on the X chromosome, which particularly involved the *Xlr* and *Magea* families (10.26%; Supplementary Fig. 13c–e).

Comparison of the imprinted genes between *Egfp*- and *Kdm4b*-PEs revealed that only six genes were significantly differentially expressed (paternally expressed genes: *Impact* and *Fthl17*; maternally expressed genes: *Gnas*, *H13*, *Xlr3b* and *Xlr4b*; Fig. 5d). Clustering analysis based on the expression of imprinted genes showed that the expression levels in *Kdm4b*-PEs were similar to those in *Egfp*-PEs rather than to those of biparental embryos (Fig. 5d). Thus, H3K9me3 demethylation does not result in restoration of expression states in paternally expressed genes.

We conducted *in vivo* transplantation experiments using *Kdm4b*-PEs. Surprisingly, at E6.5, the developmental rates of *Kdm4b*-PEs were markedly increased compared with those of *Egfp*-PEs (*Kdm4b*-PEs: 90% versus *Egfp*-PEs: 35%; $P<0.001$, Fisher's exact test; Fig. 5e,f). At E9.5, although the stages of the recovered embryos varied, *Kdm4b*-PEs retained a significantly higher developmental ability compared with controls (*Kdm4b*-PEs: 64.3% versus *Egfp*-PEs: 31.9%; $P<0.002$, Fisher's exact test; Fig. 5e,f).

However, we did not rule out the possibility that the significant improvement in *Kdm4b*-PE development resulted from restoration of the expression levels of some imprinted genes. To determine whether the improvement in developmental competency could be attributed to the gain of XCI, we constructed *Kdm4b* + si-*Rnf12*-PEs. In *Kdm4b*-PEs with si-*Rnf12* at the blastocyst stage, *Xist* expression analysis by FISH revealed that *Xist* cloud signals in control *Kdm4b*-PEs were present in 51.9% of cells, while those in *Rnf12*-knockdown *Kdm4b*-PEs were present in only 10% of cells, and most of the signals were pinpoint rather than cloud (Fig. 5g,h and Supplementary Table 8).

qPCR analysis showed that although *Xist* signals were significantly reduced in *Kdm4b*-PEs with si-*Rnf12* (12.5% of the control on average), the expression levels of *Impact*, *H13* and *Gnas*, which are expressed in response to ectopic *Kdm4b* expression (Fig. 5d), did not change when compared with those of controls (Fig. 5i). We further demonstrated that RNF12 depletion did not affect *Tsix* and *Sfmbt2* expression levels in *Kdm4b*-PEs (Fig. 5i). These results clearly indicated that RNF12 depletion led to *Xist* downregulation in *Kdm4b*-PEs, without altering the features of PEs.

Finally, *in vivo* transplantation experiments demonstrated that *Xist* repression by RNF12 depletion significantly inhibited developmental competency at E6.5 in *Kdm4b*-PEs (*Kdm4b* + si-control: 84.2% versus *Kdm4b* + si-*Rnf12*: 23.5%; $P<0.0006$, Fisher's exact test; Fig. 5j,k). Taken together, these results demonstrated that the developmental defects seen in PEs immediately after implantation could be attributed to the lack of XCI, but not to loss of expression of paternally expressed genes.

Discussion

In this study, we demonstrated that maternal imprinting of Xm, which protected against *Xist* activation by RNF12 in the preimplantation stages, was mediated by H3K9me3.

Xm-*Xist* imprints are established during oogenesis and autosomal imprinting also occur in the phases[6,10]. In many imprinted genes, DNA methylation at the promoter regions is the primary regulator and H3K9me3 modifications overlap with these regions[32]. However, it is not clear why Xm-*Xist* regions are targeted by H3K9me3, but not by DNA methylation. One of the possibilities is that during primordial germ cell development, *Xist* must be silenced to activate the inactivated allele before inducing the expression of *Dnmt3a/3l*, which encodes a *de novo* DNA methyltransferase that is activated during oogenesis[33]. Consistent with this concept, *Xist* repression begins in primordial germ cells at E10.5 (ref. 34). Thus, comparison of H3K9me3 states at promoter regions in non-growing oocytes with those in growing oocytes will greatly facilitate understanding of the molecular mechanisms of iXCI.

We found that *Kdm4b*-, *Egfp* + TSA- and *Kdm4b* + TSA-PEs did not show complete XCI at the blastocyst stage as compared with female FEs. These results suggested that other repressive marks were imposed on Xm to silence Xm-*Xist* expression. Alternatively, removal of H3K9me3 may be incomplete because demethylation at RA regions was mild (Fig. 4g). However, it is not clear why RA regions show resistance against demethylation by KDM4B. As suggested in a previous study, this mechanism may be related to the three-dimensional structure of the A-repeat, which has been reported to constitute stable regions in the *Xist* transcript[35]. Further studies using ChIP-seq and/or chromatin-conformation capture sequencing technologies in preimplantation embryos are required for comprehensive understanding of *Xist* regulation.

In ES cells, RNF12 induces *Xist* expression through degradation of REX1, which is required for suppression of *Tsix*[36]. Interestingly, we did not detect *Tsix* expression from the morula to the blastocyst stages in *in vitro*-fertilized (IVF) embryos, implying that the molecular mechanism of RNF12-mediated *Xist* activation differs between imprinted and randomly induced XCI. It is not known whether the role of RNF12 in *Xist* activation during the preimplantation stages was direct or indirect. Recent RNF12 studies reported the specific binding of RNF12 to *Smad7* in mouse ES cells[37], suggesting that signalling via transforming growth factor-β family members may be associated with imprinted *Xist* activation.

In this study, we revealed the molecular mechanisms underlying imprinting of XCI and demonstrated the role of XCI in various types of embryo development in mice. Recent studies using somatic- and ES-cloned embryos revealed that aberrant *Xist* reprogramming is a major cause of developmental failure in cloned embryos[27,28]. We found that RNF12 was highly expressed in oocytes compared with somatic and ES cells (>80-fold). Moreover, we showed that H3K9me3 levels at *Xist* promoter regions were low in ES cells and that *Xist* expression in ES-cloned embryos depended on RNF12. These data provided the first evidence that RNF12 inhibited developmental reprogramming. Therefore, the use of RNF12-depleted oocytes as recipient cells would improve cloning efficiency. However, *Xist* activation in cloned embryos may be induced by factors other than RNF12, as supported by the observation that *Xist* was still expressed at ~40% of control levels, even after marked depletion of RNF12. Consistent with this notion, a recent study has demonstrated that RNF12 is dispensable for random XCI *in vivo*[38].

Xm-*Xist* derepression from the four-cell stage could rescue developmental defects in PEs. This finding demonstrated that the primary cause of developmental failure immediately after implantation was a lack of XCI, but not a lack of expression of paternally imprinted genes. We also tested whether *Kdm4b*-PEs could extend development; however, we did not observe extended *Kdm4b*-PE development after E9.5, implying that expression of paternally imprinted genes is required for subsequent development in PEs[11,12].

Our data resolved several long-standing unanswered questions about XCI during preimplantation in various types of embryos (Supplementary Fig. 14). Moreover, given that injection of *Kdm4b* mRNA into PEs improved their developmental ability, genetic mutation leading to embryonic lethality could be rescued by transient expression of epigenomic modifiers during preimplantation phases.

Methods

Embryo manipulations. All mice were maintained and used in accordance with the Guidelines for the Care and Use of Laboratory Animals of the Japanese Association for Laboratory Animal Science and the National Research Institute for Child Health and Development (NRICHD) of Japan. All animal experiments were performed according to protocols approved by the Institutional Animal Care and Use Committee of the NRICHD (Permit Number: A2006-009).

Adult female B6D2F1 mice were purchased from Clea Japan (Tokyo, Japan) and oocytes were collected following standard methods[27]. PEs were generated using Ca-free M16 medium containing 8 mM $SrCl_2$ and Cytochalasin B (5 μg ml^{-1}) (Sigma-Aldrich, St Louis, MO, USA), and cultured KSOM (EMD Millipore, Darmstadt, Germany). Injection experiments (mRNA, short interfering RNA (siRNA) and nuclear transfer) were conducted using a Prime Tech Piezo drive (Sutter Instrument Company, Novato, CA, USA). To produce cloned embryos, nuclear-transferred oocytes were parthenogentically activated. Manipulated embryos were cultured to the developmental stages, as follows: 4-cell, 48 h; morula, 72 h; and blastocyst, 96 and 120 h after parthenogenetic activation or ICSI, respectively. All embryos were cultured at 37 °C in KSOM in an atmosphere containing 5% CO_2. In the TSA experiment, the embryos were cultured for 24 h in activation and culture media containing 50 nM TSA (Sigma-Aldrich). IVF fertilization and nuclear transfer were performed following published procedures[27]. To determine the effects of ectopic KDM4B expression on *Xist* expression in cloned embryos, doxycycline was added to ES cell culture and KSOM medium to a final concentration of 2 μg ml^{-1}. Pseudopregnant ICR mice (Clea Japan) were used as embryo recipients. At E6.5, E9.5 and E18.5, the embryos were recovered from the uterus.

***In vitro* mRNA synthesis.** The coding region of *Kdm3a* was amplified from mouse testis complementary DNA using PCR with KOD-Plus-Neo DNA polymerase (Toyobo, Osaka, Japan). Forward and reverse primers contained T7 promoter and poly(T)$_{120}$ sequences, respectively. A step-down PCR amplification method was used, following the manufacturer's instructions (Toyobo). Poly(A)-containing PCR products were subjected to *in vitro* transcription using a mMESSAGE mMACHINE T7 ULTRA Kit (Life Technologies, Carlsbad, CA, USA), following the manufacturer's instructions. To generate a *Kdm4b* DNA template for *in vitro* transcription, pCMV-SPORT6 containing the full-length *Kdm4b* mRNA was used as the PCR template (DNAFORM, Kanagawa, Japan, Clone ID 3490671). *Egfp* cDNA was cloned using the pGEM-T Easy Vector System (Promega, Madison, WI, USA) and transcribed *in vitro* using the mMESSAGE mMACHINE T7 ULTRA Kit (Life Technologies) following the manufacturer's instructions. The concentrations of the mRNAs were adjusted to 150 ng ml^{-1} (*Egfp*), 550 ng ml^{-1} (*Kdm3a*), or 450 ng ml^{-1} (*Kdm4b*) to maintain a constant number of injected mRNA molecules. The primer sequences used for generating the templates for *in vitro* transcription are shown in Supplementary Table 9.

***Rnf12* knockdown.** siRNA targeting *Rnf12* (si-Rnf12 sense 5′-GAAGUCAAAUG GAUCGCUUTT-3′ A and antisense 5′-AAAGCGAUCCAUUUGACUUCTG-3′ GC, and the negative control siRNA (si-control: 4390846) were purchased from Life Technologies. The final concentration of each siRNA was 50 ng ml^{-1}. The siRNA was injected into MII oocytes using the Piezo drive and then incubated for 6–7 h in KSOM medium at 37 °C in an atmosphere containing 5% CO_2 before mRNA injection. For the NT experiment using *Rnf12*-knockdown oocytes, oocytes were incubated for 5–6 h after siRNA injection, and NT was then conducted and activated as described above.

Immunofluorescence. Oocytes injected with mRNAs were subjected to ICSI. After 10–11 h, the zygotes were fixed with 2% paraformaldehyde (PFA) in PBS containing 0.1% polyvinyl alcohol (PBS-PVA) for 15 min at room temperature (RT). Zygotes were then permeabilized using 0.2% Triton X-100 in PBS-PVA for 15 min at RT and blocked in 1% BSA in PBS-PVA for 1 h at RT. The primary antibodies used in the assay were as follows: anti-H3K9me3 (ab8898, 1:500 dilution, Abcam, Cambridge, UK), anti-H3K9me2 (ab1220, 1:500, Abcam) and anti-H3K27me3

(07-449, 1:150, EMD Millipore). The primary antibodies were diluted with blocking solution (PBS-PVA containing 1% BSA) and the embryos were incubated overnight at 4 °C. After washing in blocking solution, the embryos were incubated for 1 h at RT with Alexa Flour 634- or 546-conjugated anti-mouse or anti-rabbit IgG secondary antibodies (1:500, Life Technologies). After the embryos were washed, the nuclei were stained with 1 μg ml^{-1} 4′,6-diamidino-2-phenylindole and the embryos were placed on a glass slide and observed with a LSM510 laser scanning confocal microscope (Carl Zeiss, Oberkochen, Germany). Signal intensities of maternal and paternal pronuclei were calculated using NIH ImageJ software (http://rsb.info.nih.gov/ij/).

In *Rnf12*-knockdown experiments, one-cell and four-cell PEs were fixed at 10–11 h (18–19 h after siRNA injection) and 48 h after activation, respectively. Anti-RNF12 (1:500, Abnova, Taipei, Taiwan) and Alexa Fluor 488-conjugated anti-mouse IgG antibodies (1:500, Life Technologies) were used as the primary and secondary antibodies, respectively. *Rnf12*-knockdown and negative-control PEs were observed under the same conditions, to assess knockdown efficiency. Signal intensities were calculated using ImageJ software.

Fluorescent *in situ* hybridization. The zona pellucida of embryos was removed using acid Tyrode solution (Sigma-Aldrich) and then fixed and permeabilized with 2% PFA-PVA containing 0.25% Triton X-100 for 10 min on ice. The samples were placed on glass slides, evaporated to dryness, dehydrated sequentially in 70 and 100% ethanol and then air-dried. Hybridization buffer containing an *Xist* probe (provided by T. Sado) was prepared using a Nick Translation Kit (Abbott, Abbott Park, IL, USA) and Cy3-dUTP (GE Healthcare Life Sciences, Fairfield, CT, USA) and was then applied to the slides. The slides were then incubated and washed as previously described[26]. Fluorescence was visualized using the LSM510.

IF combined with FISH. The zona pellucida of embryos was removed using acid Tyrode solution (Sigma-Aldrich) and fixed with 2% PFA-PVA for 15 min at RT in four-well dishes. The fixed samples were permeabilized with 0.5% Triton X-100 in PBS-PVA for 20 min on ice. After washing with PBS-PVA, the samples were blocked in 1% BSA-PBS-PVA containing 1.3 U ml^{-1} RNaseOUT (Life Technologies) for 30 min at RT. After washing, the embryos were incubated with primary antibodies (anti-CDX2 (BioGenex, San Ramon, CA, USA), diluted 1:30 and anti-H3K27me3 diluted 1:150 in blocking buffer containing 1.3 U ml^{-1} RNaseOUT) for 1 h at RT. Secondary antibody reactions were performed as described above. The samples were placed on glass slides, evaporated to dryness, dehydrated sequentially in 70 and 100% ethanol and air dried. The samples were then analysed by FISH according to the procedures described above.

Analysis of IF combined with FISH data. *Xist* cloud signals detected in three-dimensional images using *Z*-sections of the LSM Image Browser (Carl Zeiss) were judged as positive. Only cells that did not overlap at interphase were used in the analysis. Biallelic expression was defined as cells with two *Xist* cloud spots. Statistical analysis was performed using Fisher's exact test.

Gene expression analysis. Total RNA was extracted using an RNeasy Micro Kit (Qiagen, Venlo, The Netherlands) and treated with DNase following the manufacturer's instructions. mRNAs were reverse transcribed using an oligo(dT) primer and SuperScriptIII Reverse Transcriptase (Life Technologies). For quantitative gene expression analysis with high specificity, TaqMan probes (Life Technologies) were used in all assays. In four-cell stage embryos, *Xist* was assayed in triplicate and only the samples that were detected in two or three replicates were judged as positive. In morulae and blastocysts, expression of target genes was assayed in duplicate. *Gapdh* was used as the internal control in the four-cell-stage assays and *Rnf12* was used in the time-lapse assays. *Gapdh* and *Actb* (encoding β-actin) were used as internal controls at the morula and blastocyst stages. For normalization of qPCR analysis (Fig. 2b,g), the expression levels of all embryos were normalized to the average expression levels of *Egfp*-PEs. The TaqMan probes and primer sets used in this study are shown in Supplementary Table 8.

Generation of *Kdm4b*-inducible ES cell lines and ES cell culture. The XhoI- and ClaI-linearized pGEM-IRES-EGFP plasmids were inserted into the cognate sites of pPB-CAG-EBNX (provided by A. Bradley) to generate pPB-CAG-IRES-EGFP. A Tet3G fragment with BglII and XhoI cleavage sites was amplified from a pEF1a-Tet3G template (Clontech Laboratories, Mountain View, CA, USA) using PCR and inserted into pPB-CAG-IRES-EGFP, generating the vector pPB-CAG-Tet3G-IRES-EGFP. The XhoI and BamHI cleavage sites in pPB-UbC (provided by A. Bradley) were replaced with the p-TRE3G multiple cloning sites (Clontech). The *Kdm4b* coding sequence, with terminal ClaI and BamHI cleavage sites, was amplified by PCR and inserted into the corresponding sites of pPB-TRE3G, yielding pPB-TRE-Kdm4b.

The NCH.4.6 male mouse ES cell line (C57B6/N × C57B6/N), which had a normal karyotype, was electroporated with pPB-TRE-Kdm4b, pPB-CAG-Tet3G-IRES-EGFP and pCMV-hyPBase (provided by A. Bradley). All ES cells used in this study were cultured in knockout DMEM (Life Technologies) containing recombinant human leukemia inhibitory factor culture supernatant for mouse ES cell culture (Wako Pure Chemical Industries, Ltd, Osaka, Japan), as well as GlutaMAX, 2-mercaptoethanol, non-essential amino acids and 15% KSR (all from Life Technologies). Doxycycline (2 μg ml^{-1}; Sigma-Aldrich) was added to ES cell culture medium to induce ectopic KDM4B expression.

Western blotting. Cells were extracted using a stock lysis buffer containing 1 M Tris–HCl, 5 M NaCl, 10% Triton-X and protease inhibitors, and were subjected to e-PAGEL (ATTO, Amherst, NY, USA) electrophoresis. The membranes were washed in TBS containing 0.1% Tween 20 (TBS-T) and blocked in 5% skim milk in TBS-T for 1 h. The membranes were incubated with anti-KDM4B antibodies (1:500 dilution; Active Motif, Carlsbad, CA, USA) overnight at 4 °C, washed and incubated with a rabbit horseradish peroxidase-conjugated secondary antibody (1:5,000 dilution; Sigma-Aldrich) for 1 h at RT. Immunoblottings were visualized using SuperSignal chemiluminescent substrate (Thermo Scientific, Waltham, MA, USA) and an ImageQuant LAS4000 system (GE Healthcare). After capturing the images, the membranes were washed with WB Stripping Buffer (Nacalai Tesque, Kyoto, Japan) for 10 min, washed with TBS-T and incubated with an anti-β-actin antibody conjugated to fluorescein isothiocyanate (1:2,000 dilution; Sigma-Aldrich) for 1 h at RT.

ChIP analysis of K4B-ES cells. Trypsinized feeder-free ES cells (2×10^7) were collected and fixed with 1% formaldehyde. The cells were resuspended in SDS lysis buffer (ChIP Reagent, Nippon Gene Co., Ltd.) and the lysate was sonicated to fragment chromatin using a S220 Focused-ultrasonicator (Covaris, Woburn, MA, USA). The chromatin was purified by centrifugation and immunoprecipitated with Protein A-beads (Veritas Life Sciences, Ribeirão Preto, Brazil) conjugated to anti-H3K9me3 antibodies (Abcam: ab8898) or rabbit IgG (Abcam: ab37415) in Buffer A with protease inhibitor (LowCell ChIP kit, Diagenode, Denville, NJ, USA) overnight at 4 °C. The chromatin beads were washed with Buffers A and C (LowCell ChIP kit). After washing, the chromatin beads were incubated in ChIP direct elution buffer (ChIP Reagent) for 6 h at 65 °C, following incubation with 2 μl proteinase K (20 mg0 ml^{-1}) for 2 h at 55 °C. The DNA immunoprecipitated from the supernatant was purified using Agencourt AMPure XP beads (Beckman Coulter, Inc., Pasadena, CA, USA) according to the manufacturer's instructions.

ChIP combined with deep sequencing. ChIP-Seq libraries were prepared using the NEBNext ChIP-Seq Library Prep Master Mix Set and Multiplex Oligos from Illumina (New England BioLabs Inc., Ipswich, MA, USA) according to the manufacturer's instructions. Ten nanograms of ChIP or input DNA was subjected to end repair, dA-tailing and adaptor ligation, and amplified using nine cycles of PCR. The final library size was checked using a 2100 Bioanalyzer (Agilent Technologies, Santa Clara, CA, USA). After the concentration of each library was determined using qPCR with a KAPA Library Quantification Kit-Illumina/Universal system (KK4824, Kapa Biosystems, Wilmington, MA, USA), the libraries were sequenced using the HiSeq 1000 sequencing system (Illumina, San Diego, CA, USA) to generate 100 bp × 2 paired-end data.

ChIP-seq data analysis. Reads from each sample were first trimmed by removing adapter sequences and low-quality bases at ends using Trimmomatic 0.22 (http://www.usadellab.org/cms/index.php?page=trimmomatic). Approximately 115 million reads for each of the ChIP and input libraries were aligned to the mouse reference genome (mm10:http://genome.ucsc.edu/cgi-bin/hgGateway) using the Burrows-Wheeler Aligner 0.6.2. Uniquely mapped reads were selected using a custom script, converted from SAM to BAM format using SAMtools 0.1.18 and processed using Picard 1.83 to mark PCR duplicates. Reads with a mapping quality of <20 were removed using SAMtools 0.1.18. The resulting BAM files (a pair of files for ChIP and input libraries) were visualized using the Integrative Genomics Viewer (http://www.broadinstitute.org/igv/) and subjected to peak detection using the MACS algorithm implemented in Avadis NGS software (Agilent). In scatter plot analysis using 1 and 15 K4B-ES cell lines, the numbers of mapped reads were counted for 10,000-bp windows (with a sliding size of 5,000 bp). To adjust for differences in total amount of reads, the number of mapped reads in each window was transformed into reads per million format. Calculation methods are available on request.

ChIP-qPCR analysis of sperm. Sperm were obtained from BDF1 mice aged 9–12 weeks. Preparation of sperm chromatin was performed according to published protocols with modifications[39,40]. For each native ChIP experiment, 5×10^7 sperm were used. Sperm were washed twice with PBS. The pellet was suspended in PBS containing 0.5% Triton-X, 10 mM dithiothreitol (DTT) and protease inhibitor (Diagenode), and incubated on ice for 1.5 h. After washing with PBS, pelleted sperm nuclei were suspended in 400 μl PBS containing 1 mM $CaCl_2$ and 1 mM DTT, and incubated for 5 min at 37 °C. After incubation, 1 μl (2×10^6 gel units per ml) micrococcal nuclease (New England BioLabs) was added to the nuclei, which were then incubated for 5 min at 37 °C. EDTA was added to a concentration of 0.5 mM and solubilized chromatin was clarified by centrifugation for 15 min at 15,000 r.p.m. at 4 °C. The pellets were suspended in PBS containing $CaCl_2$ and DTT (at the same concentrations as used above), and treated again with micrococcal nuclease. To examine whether H3K9me3-modified nucleosomes were

present in sperm chromatin, soluble (chromatin) and insoluble (pellet) fractions were subjected to western blotting using anti-H3K9me3 antibodies (ab8898; 1:1,000), as described above.

Chromatin was incubated with Protein A beads conjugated to anti-H3K9me3 antibodies (ab8898) or rabbit IgG (ab37415) overnight at 4 °C in ChIP buffer (40 mM Tris–HCl, pH 7.5, 1 M NaCl and 10 mM EDTA). Pelleted beads were washed twice with Buffer 1 (50 mM Tris–HCl, pH 7.5, 500 mM NaCl and 10 mM EDTA) and Buffer 2 (50 mM Tris-HCL, pH 7.5, 300 mM NaCl and 10 mM EDTA). The pelleted beads were suspended in ChIP direct elution buffer and incubated with proteinase K for 2 h at 37 °C. The immunoprecipitated DNA was then purified using Agencourt AMpure XP beads.

ChIP-qPCR analysis was performed according to published methods using SYBR Green[39]. The sequences of each primer set are listed in Supplementary Table 9.

eChIP-quantitative qPCR. The zona pellucidae of the embryos were removed by acid Tyrode's solution and washed in PBS containing 0.1% PVA. The embryos were suspended in PBS containing 0.5% Triton-X, 0.5 mM DTT and protease inhibitor, and incubated on ice for 30 min. After incubation, 1 mM $CaCl_2$ was added to the buffer and samples were incubated for 5 min at 37 °C. After incubation, 0.5 μl (2×10^6 gel units per ml) micrococcal nuclease (New England BioLabs) was added to the nuclei, which were then incubated for 5 min at 37 °C. EDTA was added to a concentration of 0.5 mM and solubilized chromatin was clarified by centrifugation at 15,000 r.p.m. for 15 min at 4 °C. The same procedures were repeated one more time. Chromatin was incubated with Protein A beads conjugated to anti-H3K9me3 antibodies (ab8898) or rabbit IgG (ab37415), prepared as described above, overnight at 4 °C in ChIP buffer (40 mM Tris–HCL, pH 7.5, 1 M NaCl and 10 mM EDTA). Pelleted beads were washed twice with Buffer 1 (50 mM Tris–HCL, pH 7.5, 500 mM NaCl and 10 mM EDTA) and then with Buffer 2 (50 mM Tris–HCL, pH 7.5, 300 mM NaCl and 10 mM EDTA). The pelleted beads were then suspended in ChIP direct elution buffer and incubated with proteinase K for 2 h at 55 °C. The immunoprecipitated DNA was then purified using Agencourt AMpure XP beads.

Eluted DNA (20 μl) was divided into two aliquots; one (4 μl) was used for a SYBR Green assay targeting a major satellite and the other (16 μl) was subjected to pre-amplification using a Single Cell-to-CT kit (Ambion, Austin, TX, USA) according to the manufacturer's instructions. The number of PCR cycles at the pre-amplification step was 20. The primer and probe sequences used are shown in Supplementary Table 9.

Microarray analysis. Five *Egfp*-PE, *Kdm4b*-PE and IVF blastocysts (120 h) were lysed using ISOGEN (Nippongene) and RNA was extracted by phenol–chloroform and isopropanol precipitation. cDNA was synthesized using the Ovation RNA Amplification System V2 kit (NuGEN, West Cumbria, UK) and hybridized with SurePrint G3 Mouse GE 8x60K Microarray (Agilent Technologies). Analysis was conducted using GeneSpringV12.5 (Agilent Technologies). Transcripts were considered to be expressed if raw values were >100 and a flag was present in at least one of the groups.

References

1. Augui, S., Nora, E. P. & Heard, E. Regulation of X-chromosome inactivation by the X-inactivation centre. *Nat. Rev. Genet.* **12,** 429–442 (2011).
2. Lee, J. T. Gracefully ageing at 50, X-chromosome inactivation becomes a paradigm for RNA and chromatin control. *Nat. Rev. Mol. Cell Biol.* **12,** 815–826 (2011).
3. Wutz, A. Gene silencing in X-chromosome inactivation: advances in understanding facultative heterochromatin formation. *Nat. Rev. Genet.* **12,** 542–553 (2011).
4. Takagi, N. & Sasaki, M. Preferential inactivation of the paternally derived X chromosome in the extraembryonic membranes of the mouse. *Nature* **256,** 640–642 (1975).
5. Shin, J. *et al.* Maternal Rnf12/RLIM is required for imprinted X-chromosome inactivation in mice. *Nature* **467,** 977–981 (2010).
6. Tada, T. *et al.* Imprint switching for non-random X-chromosome inactivation during mouse oocyte growth. *Development* **127,** 3101–3105 (2000).
7. Chiba, H. *et al. De novo* DNA methylation independent establishment of maternal imprint on X chromosome in mouse oocytes. *Genesis* **46,** 768–774 (2008).
8. Marahrens, Y., Panning, B., Dausman, J., Strauss, W. & Jaenisch, R. Xist-deficient mice are defective in dosage compensation but not spermatogenesis. *Genes Dev.* **11,** 156–166 (1997).
9. Liu, N. *et al.* Genome-wide gene expression profiling reveals aberrant MAPK and Wnt signaling pathways associated with early parthenogenesis. *J. Mol. Cell Biol.* **2,** 333–344 (2010).
10. Obata, Y. & Kono, T. Maternal primary imprinting is established at a specific time for each gene throughout oocyte growth. *J. Biol. Chem.* **277,** 5285–5289 (2002).
11. Kono, T. *et al.* Birth of parthenogenetic mice that can develop to adulthood. *Nature* **428,** 860–864 (2004).
12. Kawahara, M. *et al.* High-frequency generation of viable mice from engineered bi-maternal embryos. *Nat. Biotechnol.* **25,** 1045–1050 (2007).
13. Santos, F., Peters, A. H., Otte, A. P., Reik, W. & Dean, W. Dynamic chromatin modifications characterise the first cell cycle in mouse embryos. *Dev. Biol.* **280,** 225–236 (2005).
14. Cantone, I. & Fisher, A. G. Epigenetic programming and reprogramming during development. *Nat. Struct. Mol. Biol.* **20,** 282–289 (2013).
15. Lewis, A. *et al.* Imprinting on distal chromosome 7 in the placenta involves repressive histone methylation independent of DNA methylation. *Nat. Genet.* **36,** 1291–1295 (2004).
16. Yuan, P. *et al.* Eset partners with Oct4 to restrict extraembryonic trophoblast lineage potential in embryonic stem cells. *Genes Dev.* **23,** 2507–2520 (2009).
17. Fodor, B. D. *et al.* Jmjd2b antagonizes H3K9 trimethylation at pericentric heterochromatin in mammalian cells. *Genes Dev.* **20,** 1557–1562 (2006).
18. Nakamura, T. *et al.* PGC7 binds histone H3K9me2 to protect against conversion of 5mC to 5hmC in early embryos. *Nature* **486,** 415–419 (2012).
19. Nesterova, T. B., Barton, S. C., Surani, M. A. & Brockdorff, N. Loss of Xist imprinting in diploid parthenogenetic preimplantation embryos. *Dev. Biol.* **235,** 343–350 (2001).
20. Plath, K. *et al.* Role of histone H3 lysine 27 methylation in X inactivation. *Science* **300,** 131–135 (2003).
21. Okamoto, I., Tan, S. & Takagi, N. X-chromosome inactivation in XX androgenetic mouse embryos surviving implantation. *Development* **127,** 4137–4145 (2000).
22. Barakat, T. S. *et al.* RNF12 activates Xist and is essential for X chromosome inactivation. *PLoS Genet.* **7,** e1002001 (2011).
23. Puschendorf, M. *et al.* PRC1 and Suv39h specify parental asymmetry at constitutive heterochromatin in early mouse embryos. *Nat. Genet.* **40,** 411–420 (2008).
24. Dahl, J. A. & Collas, P. A rapid micro chromatin immunoprecipitation assay (microChIP). *Nat. Protoc.* **3,** 1032–1045 (2008).
25. Turner, B. in *Mapping Protein/DNA Interactions by Cross-Linking* (2001).
26. Hoki, Y. *et al.* A proximal conserved repeat in the Xist gene is essential as a genomic element for X-inactivation in mouse. *Development* **136,** 139–146 (2009).
27. Fukuda, A. *et al.* Identification of inappropriately reprogrammed genes by large-scale transcriptome analysis of individual cloned mouse blastocysts. *PLoS ONE* **5,** e11274 (2010).
28. Inoue, K. *et al.* Impeding Xist expression from the active X chromosome improves mouse somatic cell nuclear transfer. *Science* **330,** 496–499 (2010).
29. Marks, H. *et al.* The transcriptional and epigenomic foundations of ground state pluripotency. *Cell* **149,** 590–604 (2012).
30. Karimi, M. M. *et al.* DNA methylation and SETDB1/H3K9me3 regulate predominantly distinct sets of genes, retroelements, and chimeric transcripts in mESCs. *Cell Stem Cell* **8,** 676–687 (2011).
31. Ono, Y. & Kono, T. Irreversible barrier to the reprogramming of donor cells in cloning with mouse embryos and embryonic stem cells. *Biol. Reprod.* **75,** 210–216 (2006).
32. Dindot, S. V., Person, R., Strivens, M., Garcia, R. & Beaudet, A. L. Epigenetic profiling at mouse imprinted gene clusters reveals novel epigenetic and genetic features at differentially methylated regions. *Genome Res.* **19,** 1374–1383 (2009).
33. Sasaki, H. & Matsui, Y. Epigenetic events in mammalian germ-cell development: reprogramming and beyond. *Nat. Rev. Genet.* **9,** 129–140 (2008).
34. Sugimoto, M. & Abe, K. X chromosome reactivation initiates in nascent primordial germ cells in mice. *PLoS Genet.* **3,** e116 (2007).
35. Duszczyk, M. M., Wutz, A., Rybin, V. & Sattler, M. The Xist RNA A-repeat comprises a novel AUCG tetraloop fold and a platform for multimerization. *RNA* **17,** 1973–1982 (2011).
36. Gontan, C. *et al.* RNF12 initiates X-chromosome inactivation by targeting REX1 for degradation. *Nature* **485,** 386–390 (2012).
37. Zhang, L. *et al.* RNF12 controls embryonic stem cell fate and morphogenesis in zebrafish embryos by targeting Smad7 for degradation. *Mol. Cell* **46,** 650–661 (2012).
38. Shin, J. *et al.* RLIM is dispensable for X-chromosome inactivation in the mouse embryonic epiblast. *Nature* **511,** 86–89 (2014).
39. Brykczynska, U. *et al.* Repressive and active histone methylation mark distinct promoters in human and mouse spermatozoa. *Nat. Struct. Mol. Biol.* **17,** 679–687 (2010).
40. Hammoud, S. S. *et al.* Distinctive chromatin in human sperm packages genes for embryo development. *Nature* **460,** 473–478 (2009).

Acknowledgements

We are grateful to T. Sado for critical reading of this manuscript and discussions. We thank T. Sugawara and H. Kobayashi for helpful comments; A. Bradley for providing the PiggyBac vector; K. Kusakabe, T. Kikuchi, Y. Harada, S. Kanai and Y. Takahashi for technical assistance with some experiments and analysis; and T. Kawasaki for preparation of figures. This work was supported by grants from the Ministry of Education, Culture, Sports, Science and Technology (MEXT) of Japan; a grant from the Ministry of Health, Labour and Welfare (MHLW) to H.A. and A.U.; a Grant-in-aid for Scientific

Research (21390456); a grant from JST-CREST to H.A.; and a JSPS KAKENHI Grant-in-Aid for Research Activity Start-up to A.F. (24890300).

Author contributions

A.F., K.E. and H.A. conceived and designed the study. A.F. performed the experiments and analysis of embryo manipulation, IF, FISH, qPCR, ChIP, cultured ES cells, vector construction and microarray analysis, and developed the eChIP-qPCR technique. J.T., K.H. and K.N. conducted ChIP-seq experiments and analyses. T.M. and H.A. constructed vectors and cultured ES cells. H.A. and A.U. supervised the study. A.F., K.N. and H.A. wrote the manuscript.

Additional information

Accession codes: The original data for the microarray have been deposited in the GEO at http://www.ncbi.nlm.nih.gov/geo/ (accession number: GSE53662). The original data of ChIP-seq have been deposited in DDBJ at http://cibex.nig.ac.jp/index.jsp with accession number: DRA001041.

Supplementary Information accompanies this paper at http://www.nature.com/naturecommunications

Competing financial interests: The authors declare no competing financial interests.

Reprints and permission information is available online at http://npg.nature.com/reprintsandpermissions/

How to cite this article: Fukuda, A. *et al.* The role of maternal-specific H3K9me3 modification in establishing imprinted X-chromosome inactivation and embryogenesis in mice. *Nat. Commun.* 5:5464 doi: 10.1038/ncomms6464 (2014).

ARTICLE
PUBLISHED ONLINE: 22 JUNE 2014 | DOI: 10.1038/NCHEMBIO.1552
nature chemical biology

Notch inhibition allows oncogene-independent generation of iPS cells

Justin K Ichida[1,2,9,10], Julia TCW[1–3,10], Luis A Williams[1,2], Ava C Carter[1,2], Yingxiao Shi[9], Marcelo T Moura[1,2], Michael Ziller[1,4], Sean Singh[1,2], Giovanni Amabile[5], Christoph Bock[1,4], Akihiro Umezawa[6], Lee L Rubin[1], James E Bradner[7,8], Hidenori Akutsu[6]*, Alexander Meissner[1,4]* & Kevin Eggan[1–3]*

The reprogramming of somatic cells to pluripotency using defined transcription factors holds great promise for biomedicine. However, human reprogramming remains inefficient and relies either on the use of the potentially dangerous oncogenes *KLF4* and *CMYC* or the genetic inhibition of the tumor suppressor gene *p53*. We hypothesized that inhibition of signal transduction pathways that promote differentiation of the target somatic cells during development might relieve the requirement for non-core pluripotency factors during induced pluripotent stem cell (iPSC) reprogramming. Here, we show that inhibition of Notch greatly improves the efficiency of iPSC generation from mouse and human keratinocytes by suppressing p21 in a p53-independent manner and thereby enriching for undifferentiated cells capable of long-term self-renewal. Pharmacological inhibition of Notch enabled routine production of human iPSCs without KLF4 and CMYC while leaving p53 activity intact. Thus, restricting the development of somatic cells by altering intercellular communication enables the production of safer human iPSCs.

Use of the potent oncogenes *KLF4* and *MYC* (henceforth referred to as *CMYC*) in the generation of iPSCs limits their translational utility[1,2]. Currently, elimination of these genes during human iPSC reprogramming requires suppression of p53 activity[2–16], which in turn results in the accumulation of genetic mutations in the resulting iPSCs[8]. Therefore, there remains a real need for reprogramming approaches that enable iPSC generation without the use of *KLF4* and *CMYC* while leaving p53 activity intact.

In part to address this need, several groups have undertaken chemical screens to identify small molecules that can improve reprogramming[17–21]. Thus far, the majority of active compounds are thought to improve reprogramming by inhibiting chromatin-modifying enzymes or by reinforcing the transcriptional network associated with the pluripotent state[17–22]. Consistent with their proposed mechanisms of action, these chemicals generally function in cellular intermediates that arise late in reprogramming, catalyzing their final conversion into iPSCs[19,22]. It is currently unclear whether known chemicals are sufficient for generating iPSCs from adult human cells, which are consistently more difficult to reprogram than mouse embryonic fibroblasts[23].

Given the likely need for additional reprogramming chemicals and the knowledge that most known compounds act late in this process, we reasoned that it would be valuable to identify small molecules that improve reprogramming by acting early, perhaps within the somatic cells themselves. We reasoned that one approach toward this goal would be to identify chemicals that could modulate signal transduction cascades in somatic cell populations to enrich for those cells with an enhanced capacity for reprogramming. We reasoned that if such compounds could be identified, they might expand the translational utility of chemical reprogramming.

It has been recognized that the extent of a target cell's differentiation is an important determinant of the efficiency by which it can be reprogrammed[24–26]. We therefore hypothesized that chemically driving somatic cells into a more potent 'stem cell' state might improve their reprogramming. To test this hypothesis, we chose to ask whether known chemical inhibitors of the Notch signaling pathway could aid in reprogramming.

The Notch signaling pathway is highly conserved and regulates the proliferation and differentiation of many distinct progenitor cell and stem cell types[27]. Notch ligands are generally transmembrane proteins that require contact between two cells to mediate signal transduction[28]. In skin, Notch promotes differentiation by directly activating *CDKN1A* (henceforth referred to as *p21*) expression, which in turn blocks proliferation and induces the differentiation of keratinocyte stem cell populations[29,30]. We therefore hypothesized that inhibition of Notch in keratinocytes might enhance iPSC generation by inhibiting differentiation and enriching more easily reprogrammed progenitor cells. We also felt that keratinocytes were an attractive model for testing our hypothesis because if Notch inhibition did have an effect, it could be immediately translated to the production of patient-specific iPSCs[31,32].

Here, we show that Notch inhibition improves the efficiency of iPSC generation from mouse and human keratinocytes by suppressing p21 and thereby enriching undifferentiated cells with increased reprogramming potential. In addition, pharmacological inhibition of Notch enabled the efficient production of human iPSCs without *KLF4* and *CMYC* while leaving p53 activity intact, resulting in the production of safer human iPSCs.

[1]Harvard Stem Cell Institute, Department of Stem Cell and Regenerative Biology, Harvard University, Cambridge, Massachusetts, USA. [2]Howard Hughes Medical Institute, Stanley Center for Psychiatric Research, Cambridge, Massachusetts, USA. [3]Department of Molecular and Cellular Biology, Harvard University, Cambridge, Massachusetts, USA. [4]Broad Institute of MIT and Harvard, Cambridge, Massachusetts, USA. [5]Harvard Stem Cell Institute, Harvard Medical School, Boston, Massachusetts, USA. [6]Department of Reproductive Biology, National Research Institute for Child Health and Development, Tokyo, Japan. [7]Department of Medical Oncology, Dana-Farber Cancer Institute, Boston, Massachusetts, USA. [8]Department of Medicine, Harvard Medical School, Boston, Massachusetts, USA. [9]Department of Stem Cell Biology and Regenerative Medicine, University of Southern California, Los Angeles, California, USA. [10]These authors contributed equally to this work. *e-mail: akutsu-h@ncchd.go.go.jp, alexander_meissner@harvard.edu or keggan@scrb.harvard.edu

RESULTS

DAPT treatment promotes keratinocyte reprogramming

Notch signaling is activated by the γ-secretase complex, which cleaves the membrane-tethered Notch receptor upon ligand binding and generates a free intracellular domain that can translocate to the nucleus and modulate transcription[27]. It has previously been shown that the γ-secretase inhibitor DAPT (**Fig. 1a**) can block Notch signaling in mouse keratinocytes[33]. As expected, 10 μM DAPT treatment of both neonatal mouse and human keratinocytes transduced with the iPSC reprogramming factors increased the abundance of the full-length Notch receptor, reduced levels of cleaved Notch intracellular domain (**Supplementary Results**, **Supplementary Fig. 1a**) and decreased expression of the Notch-target genes *Hey1*, *Hes1*, *Hes5* and *Col6a1* (**Supplementary Fig. 1b**).

To determine whether inhibition of Notch could increase the efficiency of reprogramming, we used *Pou5f1* (henceforth referred to as *Oct4*), *Sox2*, *Klf4* and *cMyc* to transduce *Oct4*::GFP mouse or human keratinocytes and cultured the resulting cells for 25 d either in the presence or absence of DAPT. We found that the addition of 10 μM DAPT led to a fourfold increase in the number of resulting *Oct4*::GFP+ mouse and NANOG+/TRA-1-81+ human iPSC colonies (**Fig. 1b**).

We wondered whether this increase in reprogramming activity might allow the generation of iPSCs from keratinocytes without *Klf4* and *cMyc*. Indeed, although transduction of *Oct4* and *Sox2* alone were not sufficient to induce keratinocyte reprogramming, *Oct4* and *Sox2* combined with DAPT treatment routinely yielded mouse and human iPSC colonies (**Fig. 1c,d** and **Supplementary Fig. 2a**). This effect was specific to *Oct4*- and *Sox2*-transduced cells because other two-factor combinations did not yield iPSCs in the presence of DAPT (**Fig. 1c**).

To determine whether these putative iPS cell lines were pluripotent, we subjected them to a 'scorecard' assay for pluripotency that we recently developed[34]. We found that these cell lines were indeed composed of pluripotent cells and that they performed comparably to human embryonic stem cells in their expression of pluripotency-associated genes and differentiation propensities (**Supplementary Fig. 2b,c**). To further confirm their differentiation capacity, we also injected the *OCT4*, *SOX2*+ DAPT human cells into immunocompromised mice and found that they readily formed teratomas containing differentiated cells (**Fig. 1e**). Moreover, when injected into blastocysts, the *Oct4*, *Sox2*+ DAPT mouse cells contributed to the germline, producing chimeric mice (**Supplementary Fig. 2d,e**).

Many applications of iPSCs would require the DAPT-dependent generation of *KLF4*- and *CMYC*-free iPSCs from adult keratinocytes. Therefore, we determined whether DAPT treatment increased the reprogramming potential of adult human keratinocytes. As with mouse and human neonatal keratinocytes, we found that DAPT treatment of *KLF4*-, *SOX2*-, *OCT4*- and *CMYC*-transduced adult human keratinocytes markedly improved their rate of reprogramming (**Supplementary Fig. 2f**) and also enabled the generation of iPSCs with just *OCT4* and *SOX2* (**Fig. 1f** and **Supplementary Fig. 2g**). The scorecard assay again verified that these two-factor iPSCs were pluripotent (**Supplementary Fig. 2b,c**). Together, these results demonstrate that DAPT reliably enables the generation of bona fide mouse and human iPSCs from keratinocytes without *KLF4* and *CMYC*.

Notch inhibition promotes reprogramming

Our results thus far suggest that antagonizing Notch signaling in keratinocytes may promote their conversion into iPSCs. To begin verifying that NOTCH was indeed the functional target of DAPT during reprogramming, we tested a structurally distinct γ-secretase inhibitor, DBZ[35] (**Fig. 2a**), for activity in iPSC generation. When we treated human keratinocytes with DBZ, we observed

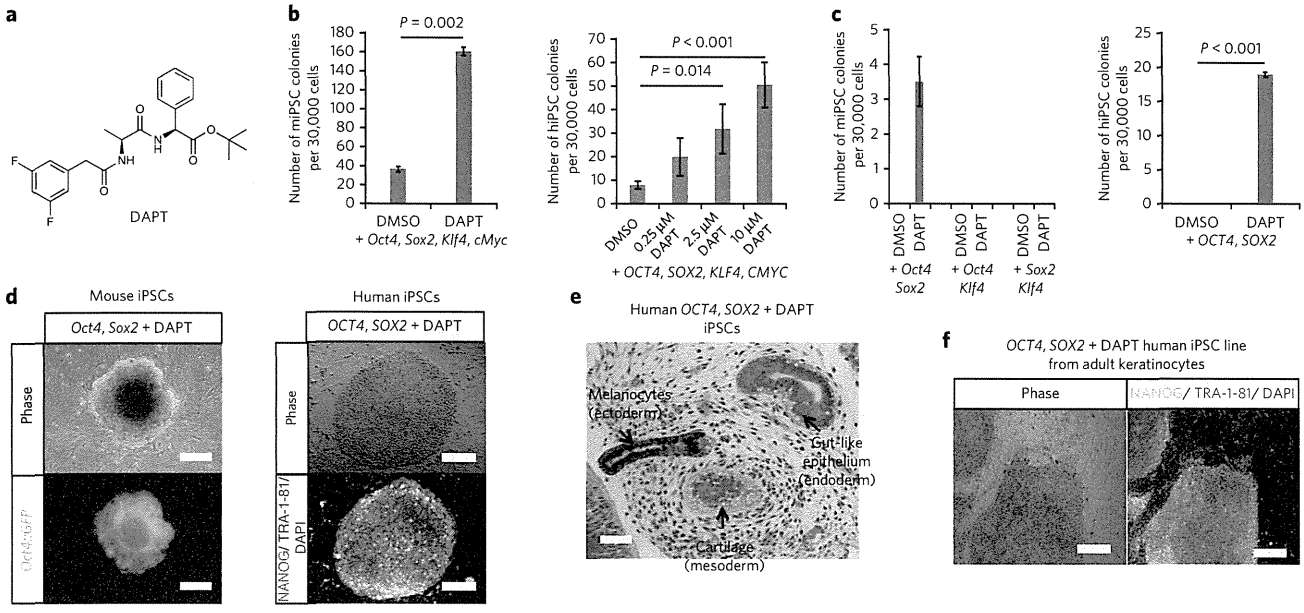

Figure 1 | DAPT treatment promotes mouse and human keratinocyte reprogramming. (**a**) Chemical structure of DAPT. (**b**) The efficiency of iPSC generation from mouse (left) and human (right) keratinocytes transduced with *Oct4*, *Sox2*, *Klf4* and *cMyc* with DMSO or DAPT treatment (DAPT used at 10 μM in mouse experiment). (**c**) The efficiency of iPSC generation from mouse (left) and human (right) keratinocytes transduced with all combinations of two reprogramming factors with DMSO or 2.5 μM DAPT treatment from days 1-18 after transduction. (**d**) A P0 mouse and human iPSC colony generated using *OCT4*, *SOX2* and DAPT. Scale bars, 100 μm. (**e**) Teratoma generated by iPSCs derived from human neonatal kerationcytes using *OCT4*, *SOX2* and DAPT. Scale bar, 50 μm. (**f**) NANOG+/TRA-1-81+ iPSC line generated from human adult keratinocytes using *OCT4*, *SOX2*+ DAPT. Scale bars, 100 μm. For all experiments, error bars represent the s.d. between two or three biological replicates, and statistical significance was determined using a two-tailed homoscedastic Student's *t*-test.

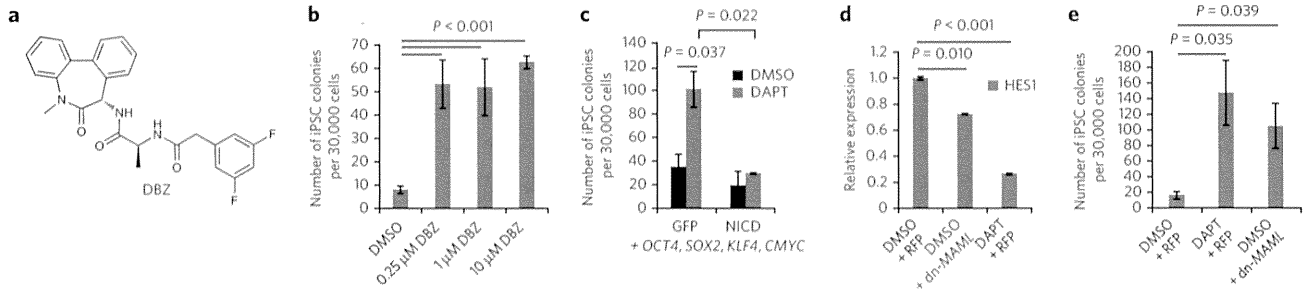

Figure 2 | γ-secretase inhibition promotes reprogramming by blocking Notch signaling. (**a**) Chemical structure of DBZ. (**b**) The efficiency of NANOG+/TRA-1-81+ iPSC generation from human neonatal keratinocytes transduced with *OCT4*, *KLF4*, *SOX2* and *CMYC* and treated with different concentrations of DBZ from days 1–18 after transduction. (**c**) The efficiency of NANOG+/ TRA-1-81+ iPSC generation from human neonatal keratinocytes transduced with *OCT*, *SOX2*, *KLF4* and *CMYC* and GFP or NOTCH intracellular domain (NICD) and treated with DMSO or 10 μM DAPT from days 1–18 after transduction. Cells were transduced with NOTCH ICD or GFP lentivirus 1 day after transduction with the reprogramming factors. (**d**) qPCR analysis of expression levels of NOTCH-dependent gene HES1 in human neonatal keratinocytes transduced with dominant-negative MASTERMIND-LIKE-1 (dn-*MAML1*) or RFP. (**e**) The efficiency of NANOG+/TRA-1-81+ iPSC generation from human neonatal keratinocytes transduced with *OCT*, *SOX2*, *KLF4* and *CMYC* and RFP or dn-*MAML1* and treated with DMSO or 10 μM DAPT from days 1–18 after transduction. For all experiments, error bars represent the s.d. between two or three biological replicates, and statistical significance was determined using a two-tailed homoscedastic Student's *t*-test.

reductions in the levels of the intracellular domain of the NOTCH receptor (**Supplementary Fig. 1a**) and the NOTCH-dependent genes *HES1* and *HES5* (**Supplementary Fig. 3a**), indicating that DBZ administration inhibited NOTCH signaling. Consistent with the notion that NOTCH inhibition increases the rate of reprogramming, DBZ stimulated the formation of human iPSC colonies (**Fig. 2b**).

Both DBZ and DAPT could have effects on the processing of unidentified γ-secretase substrates that are distinct from NOTCH, which might also affect reprogramming efficiency. If the beneficial effects of DAPT on reprogramming were being mediated through the specific inhibition of NOTCH signaling rather than through some other target of γ-secretase, then we reasoned that constitutive activation of NOTCH signaling should eliminate the beneficial effect

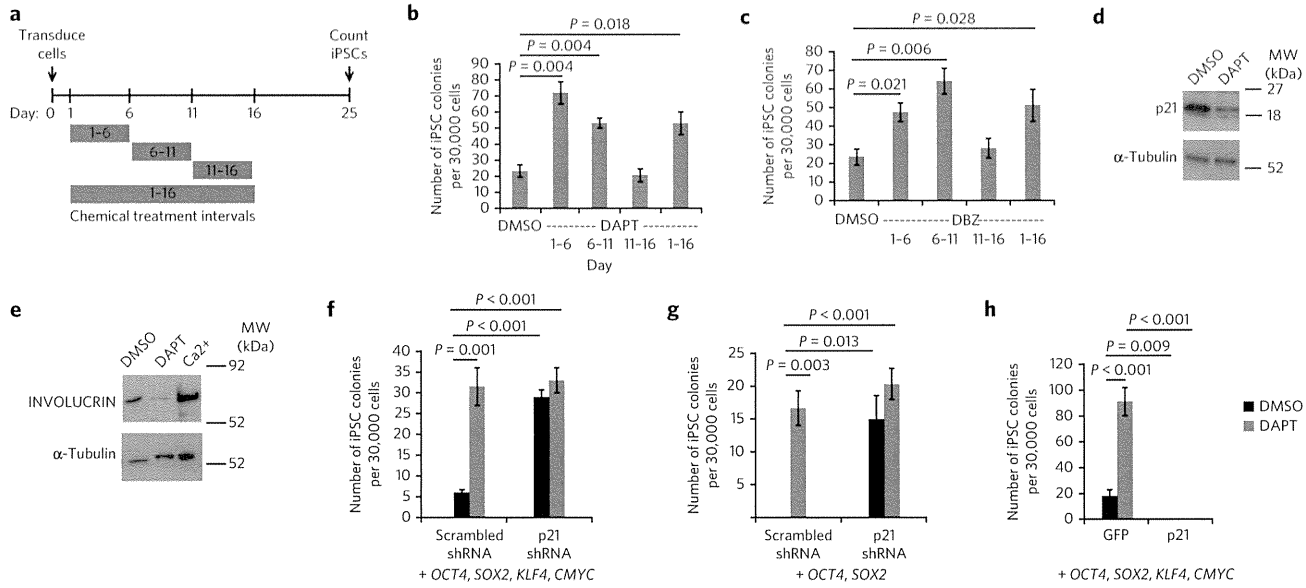

Figure 3 | Notch inhibition promotes keratinocyte reprogramming by suppressing p21. (**a**) Schematic of the DAPT treatment time course on human neonatal keratinocytes. (**b**,**c**) Efficiency of NANOG+/TRA-1-81+ iPSC generation from human neonatal keratinocytes transduced with *OCT4*, *SOX2*, *KLF4* and *CMYC* and treated with intervals of 10 μM DAPT (**b**) or 2 μM DBZ (**c**). (**d**) Western blot for p21 in human neonatal keratinocytes transduced with *OCT4* and *SOX2* and treated with DMSO or 10 μM DAPT. The full blot is shown in **Supplementary Figure 7c**. (**e**) Western blot for INVOLUCRIN in human neonatal keratinocytes treated with DMSO, 10 μM DAPT or 1.2 mM calcium chloride for 6 d. Calcium was used as a positive control to induce keratinocyte differentiation. The full blot is shown in **Supplementary Figure 7d**. (**f**) Efficiency of NANOG+/TRA-1-81+ iPSC generation from human neonatal keratinocytes transduced with *OCT4*, *KLF4*, *SOX2* and *CMYC* and a scrambled shRNA or a p21 shRNA at day 0 of reprogramming. DAPT was added at 10 μM. (**g**) Efficiency of NANOG+/TRA-1-81+ iPSC generation from human neonatal keratinocytes transduced with *OCT4* and *SOX2* and a scrambled shRNA control or a p21 shRNA at day 0 of reprogramming. DAPT was added at 2.5 μM. (**h**) Efficiency of NANOG+/TRA-1-81+ iPSC generation from human neonatal keratinocytes transduced with *OCT*, *SOX2*, *KLF4* and *CMYC* and GFP or p21 and treated with DMSO or 10 μM DAPT from days 1–18 after transduction. For all experiments, error bars represent the s.d. between two or three biological replicates, and statistical significance was determined using a two-tailed homoscedastic Student's *t*-test.

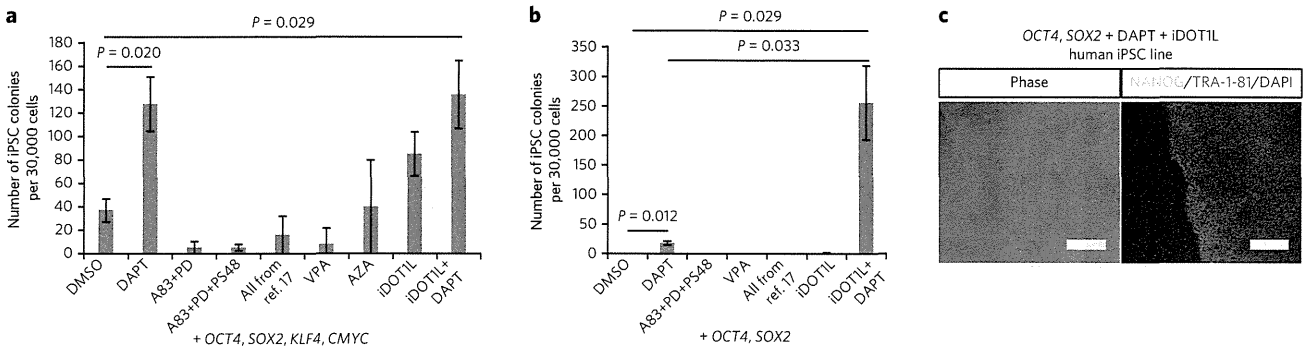

Figure 4 | Highly efficient reprogramming with NOTCH and DOT1L inhibition. (**a**) Comparison of NANOG+/TRA-1-81+ iPSC generation from *OCT4*, *SOX2*, *KLF4* and *CMYC*-transduced human neonatal keratinocytes using 10 μM DAPT versus other published reprogramming chemicals. A83, A8301 (0.5 μM); PD, PD0325901 (0.5 μM); 'All from ref. 17', A8301 (0.5 μM), PD0325901 (0.5 μM), PS48 (5 μM), sodium butyrate (0.25 mM), Parnate (2 μM) and CHIR99021 (3 μM); AZA, 5-aza-cytidine (0.5 μM); VPA, valproic acid (0.5 mM); iDOT1L, EPZ004777 (3 μM). (**b**) Comparison of NANOG+/TRA-1-81+ iPSC generation from *OCT4*- and *SOX2*- transduced human neonatal keratinocytes using 2.5 μM DAPT versus other published reprogramming chemicals. (**c**) iPSC line generated from human neonatal keratinocytes using *OCT4*, *SOX2*, DAPT and iDOT1L. Scale bars, 100 μm. For all experiments, error bars represent the s.d. between two or three biological replicates, and statistical significance was determined using a two-tailed homoscedastic Student's *t*-test.

of DAPT. Consistent with this notion, we found that overexpression of the NOTCH intracellular domain (**Supplementary Fig. 3b**) stimulated the expression of NOTCH-target genes (**Supplementary Fig. 3c**) and completely blocked the positive effects of DAPT on reprogramming (**Fig. 2c**). Conversely, we reasoned that antagonizing the transcriptional activity of NOTCH should increase the rate of keratinocyte reprogramming. Indeed, when we suppressed NOTCH activity by overexpressing a dominant-negative form of *MAML1* (**Fig. 2d**), a transcriptional co-activator for NOTCH[36,37], we observed an increase in iPSC generation from keratinocytes transduced with all four reprogramming factors (**Fig. 2e**). Therefore, we conclude that the inhibition of NOTCH signaling promotes the reprogramming of both human and mouse keratinocytes.

To understand how Notch inhibition promotes iPSC generation, we first determined when in the reprogramming process it was required. We treated mouse keratinocytes with DAPT either before or both before and after transduction with reprogramming factors. Although treatment both before and after transduction yielded a fourfold increase in iPSC generation, we found that pretreatment alone resulted in a 2.5-fold enhancement in reprogramming efficiency (**Supplementary Fig. 4a**). To more precisely pinpoint the effective post-transduction treatment window, we transduced human keratinocytes with *KLF4*, *OCT4*, *SOX2* and *CMYC* and administered DAPT or DBZ from days 1–6, 6–11, 11–16 or 1–16 after viral infection (**Fig. 3a–c**). Chemical inhibition of NOTCH signaling was most effective during early time points, increasing iPSC generation when used from days 1–6 and 6–11 (**Fig. 3b,c**). In contrast, a later treatment from days 11–16 had little effect on reprogramming (**Fig. 3b,c**). Together, these results indicate that Notch inhibition can act on the starting keratinocytes and at early time points just after the initiation of transcription factor overexpression to enhance reprogramming.

Notch inhibition acts by suppressing p21 expression

One way that Notch inhibition could promote iPSC formation is by activating the expression of the reprogramming transcription factors from their endogenous loci. However, when we treated human keratinocytes with DAPT and analyzed their gene expression, we found that levels of *KLF4*, *OCT4* and *CMYC* actually decreased, and *SOX2* levels did not change (**Supplementary Fig. 4b**).

In the mammalian epidermis, Notch signaling functions as a switch that directly activates *p21* transcription, which in turn forces keratinocytes to exit the cell cycle and begin differentiating[38]. To determine whether chemical inhibition of Notch signaling in keratinocytes might be enhancing their reprogramming potential by suppressing *p21*, we measured p21 levels in human keratinocytes in the presence and absence of DAPT. Consistent with previous reports[38], we found that Notch inhibition decreased the levels of *p21* mRNA and protein in these cells (**Fig. 3d** and **Supplementary Fig. 4c**). In addition, DAPT treatment slightly decreased the level of Flag-tagged p21 protein expressed by an exogenous retrovirus, indicating that Notch may also regulate p21 after transcription (**Supplementary Fig. 4d,e**). Consistent with these observations, Notch inhibition suppressed expression of INVOLUCRIN, which is expressed in more differentiated keratinocytes (**Fig. 3e**).

To verify that Notch inhibition promotes iPSC reprogramming by suppressing p21, we performed two-factor (*Oct4* and *Sox2*) and four-factor reprogramming in keratinocytes with p21 siRNA and shRNA in the presence or absence of DAPT. Mouse keratinocytes transduced with *Klf4*, *Sox2*, *Oct4* and *cMyc* showed a similar increase in iPSC generation when treated with either 2.5 μm DAPT or p21 siRNA (**Supplementary Fig. 4f**). The efficiency of reprogramming with these two methods was not measurably different (**Supplementary Fig. 4f**), and treating with DAPT in the presence of the p21 siRNA did not produce a demonstrable increase in iPSC formation (**Supplementary Fig. 4f**). Similarly, suppression of p21 by shRNA (**Supplementary Fig. 4g,h**) enabled the generation of iPSCs from human keratinocytes transduced with two or four factors at rates equivalent to DAPT treatment (**Fig. 3f,g**). Again, supplementing p21 knockdown with DAPT treatment did not result in an increase in iPSC formation (**Fig. 3f,g**). These results indicate that p21 suppression and DAPT have similar effects on iPSC generation from keratinocytes and that DAPT does not provide an additional advantage over p21 suppression alone.

If Notch inhibition and p21 suppression indeed blocks keratinocyte differentiation, the p21-treated keratinocytes would be predicted to display an increase in their long-term proliferative capacity[39]. The ability to form large colonies on collagen demonstrates the ability of keratinocytes to self-renew extensively and is a functional property unique to undifferentiated cells of this lineage[39]. In contrast, differentiated keratinocytes senesce after only a few rounds of division and do not form colonies[39]. DAPT treatment of human keratinocytes for 6 d markedly increased the number of cells capable of forming large colonies when cultured for an additional 14 d in the absence of the chemical (**Supplementary Fig. 4i**). The resulting fourfold increase in colony formation rate

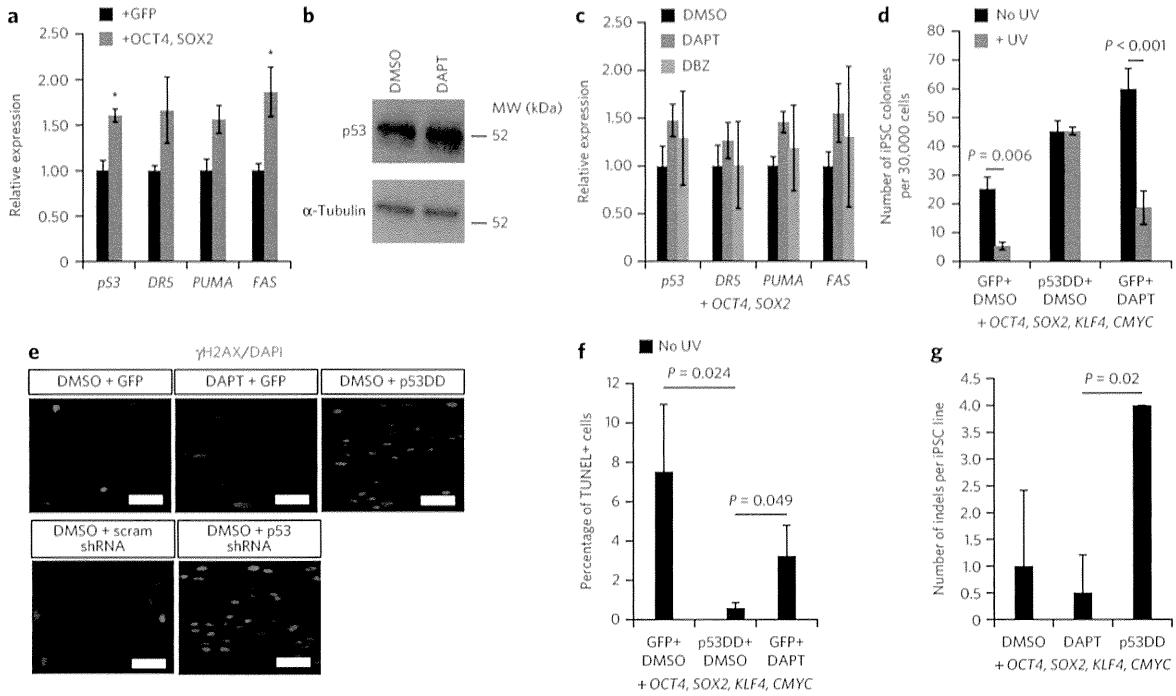

Figure 5 | NOTCH inhibition suppresses p21 without reducing p53 activity. (**a**) qPCR analysis of p53-dependent genes in human neonatal keratinocytes 3 d after transduction of GFP or *OCT4* and *SOX2*. (**b**) Western blot of p53 levels in human neonatal keratinocytes with DMSO or 10 μM DAPT treatment for 3 d. The full blot is shown in **Supplementary Figure 7g**. (**c**) qPCR analysis of p53-dependent genes after 10 μM DAPT or 2 μM DBZ treatment for 3 d in *OCT4*, *SOX2*-transduced human keratinocytes. (**d**) The efficiency of NANOG+/TRA-1-81+ iPSC generation in *OCT4*, *SOX2*, *KLF4* and *CMYC*-transduced human neonatal keratinocytes transduced with p53DD or GFP with or without exposure to UV irradiation. (**e**) γH2AX immunostaining in human neonatal keratinocytes 10 d after transduction with *OCT4*, *SOX2*, *KLF4* and *CMYC* and treatment with DAPT, p53DD or p53 shRNA. Scale bars, 50 μm. (**f**) The percentage of TUNEL-positive cells in human neonatal keratinocyte reprogramming cultures with active or inactive p53 (p53DD expression) 10 d after transduction with *OCT4*, *SOX2*, *KLF4* and *CMYC*. (**g**) The number of insertions or deletions (indels) per iPSC line derived under normal, DAPT or p53DD conditions, as determined by array comparative genomic hybridization (CGH). For all experiments, error bars represent the s.d. between two biological replicates, and statistical significance was determined using a two-tailed homoscedastic Student's *t*-test. $^*P < 0.05$.

was similar in magnitude to the elevation in iPSC generation with DAPT treatment (**Fig. 1b**). To determine whether this increased self-renewal capacity was indeed promoting reprogramming, we transduced keratinocytes with p21 to limit their replication and attempted to reprogram them either with or without DAPT. The forced p21 expression severely impaired the self-renewal potential of the keratinocytes (**Supplementary Fig. 4j**) and inhibited iPSC formation after transduction with the four reprogramming factors and treatment with DAPT (**Fig. 3h**).

Because Notch inhibition does not promote fibroblast replication[40], if this is the mechanism by which DAPT improves reprogramming, we would not expect chemical treatment to affect mouse embryonic fibroblast[41] reprogramming[41]. Indeed, DAPT treatment of MEFs transduced with all four reprogramming factors did not affect the rate of iPSC generation (**Supplementary Fig. 4k**). Together, these results demonstrate that Notch inhibition promotes iPSC generation from keratinocytes by repressing their differentiation and enhancing their long-term replicative potential through p21 suppression.

Efficient reprogramming with Notch and DOT1L inhibition

Knowing that Notch inhibition enhances iPSC generation through this unique mechanism, we next wanted to compare its activity to previously described reprogramming molecules that act through other mechanisms[17,42–44] and identify any that DAPT might synergize with. When we transduced human neonatal keratinocytes with *KLF4*, *SOX2*, *OCT4* and *CMYC* and treated them with various combinations of compounds shown to enhance reprogramming in other reports, including an activator of 3′-phosphoinositide-dependent kinase-1 (ref. 17); inhibitors of TGF-β, MEK and GSK3β signaling[17]; histone deacetylase inhibitors[17,42]; histone methyltransferase inhibitors[17,44]; and a DNA methyltransferase inhibitor[43], we found that DAPT treatment was the most potent at enhancing reprogramming (**Fig. 4a**). This remained true when we attempted reprogramming with only *OCT4* and *SOX2* (**Fig. 4b**).

However, an inhibitor of the histone methyltransferase DOT1L (iDOT1L) synergized *OCT4*, *SOX2* and DAPT to elevate the rate of iPSC generation by tenfold over the rate with *OCT4*, *SOX2* and DAPT alone, making it even more efficient than four-factor reprogramming either with or without DAPT (**Fig. 4b**). The *OCT4*+ *SOX2*+ DAPT+ iDOT1L colonies could be readily expanded and maintained NANOG and TRA-1-81 expression (**Fig. 4c**). These data indicate that Notch inhibition is a potent enhancer of reprogramming in keratinocytes that can synergize with chromatin-modifying compounds to induce pluripotency at a high efficiency with only *OCT4* and *SOX2*.

Notch inhibition does not compromise p53 activity

Previous studies of p53 and p21 in reprogramming have suggested that ectopic overexpression of reprogramming transcription factors can activate p53, which then induces either apoptosis or the expression of p21, thus inhibiting reprogramming[3,6]. Because suppression of the p53 pathway greatly facilitates iPSC generation, this approach has become an important part of reprogramming methods that reduce or eliminate integrating exogenous transcription factors[3,4]. However, because p53 inhibition allows the accumulation of

genetic mutations during reprogramming[8], alternative approaches for increasing reprogramming efficiencies would be desirable. We therefore next asked whether Notch inhibition promotes reprogramming through a p53-dependent or p53-independent pathway by analyzing the effects of DAPT and DBZ treatment on p53 and its target genes. First, we confirmed the finding that transduction with the iPSC reprogramming factors stimulated p53 activity (**Fig. 5a**). Chemical inhibition of Notch signaling in both human and mouse keratinocytes did not reduce the expression of p53 at the protein or mRNA level either before or after transduction with the reprogramming factors (**Fig. 5b,c** and **Supplementary Fig. 5a,b**). Moreover, transcriptional analysis of DAPT-treated human and mouse keratinocytes revealed that the mRNA levels of the p53 target genes *Tnfrsf10b* (also known as *Dr5*), *Bbc3* (also known as *Puma*) and *Fas* were not decreased (**Fig. 5c** and **Supplementary Fig. 5a,b**), supporting the notion that p53 activity was not suppressed by Notch inhibition.

To further confirm that DAPT treatment did not suppress p53 activity, we performed reprogramming experiments with and without DAPT after UV irradiation. UV exposure causes DNA damage, which in turn reduces reprogramming efficiencies by inducing p53-dependent apoptosis[8]. However, p53-deficient cells are resistant to the negative effects of UV irradiation on reprogramming[8]. Therefore, if p53 activity was maintained in DAPT-treated cultures, then we would expect a sharp decrease in reprogramming efficiency after UV irradiation. As a control for p53 deficiency, we performed four-factor reprogramming with or without UV irradiation using keratinocytes in which we overexpressed a dominant-negative form of p53 (p53DD)[3] that suppressed p53 activity, as evidenced by a decrease in the expression levels of p53-dependent target genes (**Supplementary Fig. 5c**). As expected, UV exposure did not affect the rate of iPSC generation when p53DD was expressed, functionally demonstrating that p53 activity was indeed impaired (**Fig. 5d**). In contrast, in the absence of p53DD overexpression, UV exposure sharply reduced the number of iPSCs generated in DMSO-treated cultures (**Fig. 5d**). Similarly, UV irradiation severely diminished the number of iPSC colonies in DAPT-treated cultures, again suggesting that Notch inhibition does not suppress p53 activity during reprogramming (**Fig. 5d**).

Although the difference in reprogramming efficiency in p53-deficient versus DAPT-treated keratinocytes was clearly evident when UV irradiation was used to induce DNA damage, we next determined whether DNA damage was measurably influenced by DAPT treatment under normal reprogramming conditions. To test this, we quantified phosphorylated histone H2AX (γH2AX) expression in four-factor-transduced human keratinocytes treated with DAPT, p53DD or p53 shRNA. Histone H2AX becomes phosphorylated in response to double-stranded DNA breaks, making it a reliable marker of DNA damage[8]. Pan-nuclear γH2AX expression results from replication-induced damage and could indicate insults sustained during reprogramming[8]. We found that 10 d after transduction, pan-nuclear γH2AX staining was greatly elevated in cultures treated with p53DD or p53 shRNA, which is consistent with a previous study in which elevated rates of DNA damage were observed in p53-deficient cells during reprogramming and in the resulting iPSCs[8] (**Fig. 5e** and **Supplementary Fig. 5d–f**). The DAPT-treated cells, however, maintained low cell numbers with pan-nuclear γH2AX expression that were similar to numbers in the control cultures (**Fig. 5e** and **Supplementary Fig. 5f**). These results suggest that, in contrast to p53 deficiency, DAPT treatment did not promote the survival and reprogramming of cells with DNA damage.

To confirm that Notch inhibition does not prevent the apoptosis of compromised cells during reprogramming, we measured the fraction of TUNEL-positive nuclei in DAPT-treated cultures. Despite high rates of DNA damage in the p53-deficient reprogramming cultures, the percentage of TUNEL-positive nuclei was greatly reduced compared to the percentage in a wild-type control, indicating that inactivation of p53 permitted the survival of cells with compromised genomes (**Fig. 5f**). In contrast, the percentage of TUNEL-positive cells was not reduced after DAPT treatment (**Fig. 5f**).

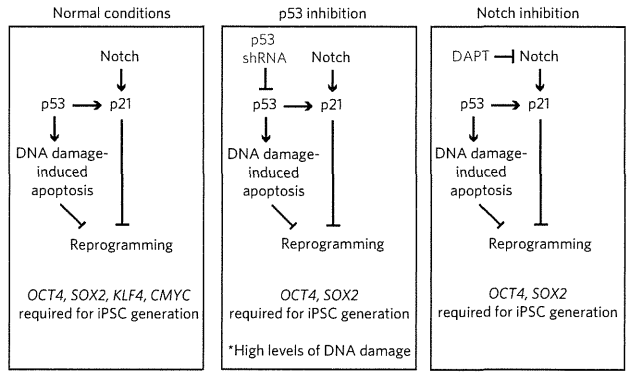

Figure 6 | Model of iPSC generation from human keratinocytes. Notch inhibition allows the production of safer oncogene-free iPSCs by suppressing p21 in a p53-independent manner.

To determine whether DAPT enabled the efficient generation of iPSCs that displayed improved genomic integrity relative to their counterparts made through p53 suppression, we measured the copy number variation in iPSC lines made with DAPT or p53DD. Consistent with the γH2AX and TUNEL staining results, we found that iPSC lines derived in the presence of p53DD had an average of four indels per line, whereas iPSCs derived with a control GFP vector or 10 μm DAPT contained only 1 or 0.5 indels per line, respectively (**Fig. 5g** and **Supplementary Fig. 6**). Together, these experiments show that DNA damage is present during normal reprogramming conditions and that inhibition of p53 allows cells with damaged genomic material to persist. In contrast, Notch inhibition enhances reprogramming without compromising genomic integrity or promoting the survival of iPSCs that have undergone DNA damage.

DISCUSSION

In summary, our findings suggest that signaling through the Notch pathway is a major impediment to the early stages of the reprogramming of both mouse and human keratinocytes into iPSCs (**Fig. 6**). Notably, the mechanism by which Notch signaling most likely inhibits reprogramming of mouse and human cells is by activating p21 independently of p53. Consistent with this hypothesis, treatment of reprogramming cultures with the γ-secretase inhibitors DAPT and DBZ reduced the levels of intracellular Notch and increased colony-forming potential, leading to an increase in the rate of iPSC formation. Suppression of p21 expression by siRNA and shRNA was sufficient to replace Notch inhibition in reprogramming, and exogenous p21 blocked the beneficial effects of DAPT. Notably, the resulting improvement in reprogramming activity did not come at the expense of a reduction in p53 activity or increased genomic instability (**Fig. 6**).

Our findings have immediate and practical ramifications for the improved production of patient-specific human iPSCs. When taken together, our studies show that through pharmacological inhibition of NOTCH, it is routinely possible to produce human iPSCs with only *OCT4* and *SOX2*, rendering *CMYC* and *KLF4* dispensable and thereby reducing the oncogenic potential of the resulting cells. Furthermore, our findings enabled *CMYC*- and *KLF4*-free iPSC production without inhibition of p53 or its target genes involved in apoptosis, allowing proapoptotic pathways that ensure genomic integrity to be engaged[8,10,11]. Thus, in this approach, the production

of oncogene-free iPSC lines does not come at the expense of an increase in mutational load[8,10,11,45].

Studies using nuclear transplantation and defined transcription factors have shown that nuclei become less amenable to reprogramming as they advance developmentally[24–26]. Our study demonstrates that intercellular communication in somatic cultures can cause them to differentiate and lose their reprogramming potential but with small-molecule treatment, it is possible to force them to remain in an undifferentiated, highly reprogrammable state. This approach synergized potently with chemical inactivation of the histone H3 methyltransferase DOT1L, allowing two-factor reprogramming at higher efficiency than with four transcription factors. This indicates that although histone methyltransferase inhibition had almost no effect on the reprogramming of differentiated keratinocytes, it had a profound ability to enhance the reprogramming of undifferentiated keratinocytes. Thus, somatic cells at different developmental stages respond differentially to chromatin-modifying signals during reprogramming. The combined chemical inhibition of NOTCH and DOT1L provides a new approach for boosting the reprogramming potential of keratinocytes and is an attractive starting point for the identification of a small-molecule reprogramming cocktail for human cells.

Accession numbers. Gene Expression Omnibus. Microarray data have been submitted to the GEO repository with accession number GSE35090.

Received 24 September 2013; accepted 13 May 2014; published online 22 June 2014; corrected after print 29 July 2014 and 14 August 2014

METHODS

Methods and any associated references are available in the online version of the paper.

References

1. Aoi, T. *et al.* Generation of pluripotent stem cells from adult mouse liver and stomach cells. *Science* **321**, 699–702 (2008).
2. Nakagawa, M. *et al.* Generation of induced pluripotent stem cells without Myc from mouse and human fibroblasts. *Nat. Biotechnol.* **26**, 101–106 (2008).
3. Kawamura, T. *et al.* Linking the p53 tumour suppressor pathway to somatic cell reprogramming. *Nature* **460**, 1140–1144 (2009).
4. Okita, K. *et al.* A more efficient method to generate integration-free human iPS cells. *Nat. Methods* **8**, 409–412 (2011).
5. Son, M.J. *et al.* Nicotinamide overcomes pluripotency deficits and reprogramming barriers. *Stem Cells* **31**, 1121–1135 (2013).
6. Hong, H. *et al.* Suppression of induced pluripotent stem cell generation by the p53-p21 pathway. *Nature* **460**, 1132–1135 (2009).
7. Utikal, J. *et al.* Immortalization eliminates a roadblock during cellular reprogramming into iPS cells. *Nature* **460**, 1145–1148 (2009).
8. Marión, R.M. *et al.* A p53-mediated DNA damage response limits reprogramming to ensure iPS cell genomic integrity. *Nature* **460**, 1149–1153 (2009).
9. Li, H. *et al.* The Ink4/Arf locus is a barrier for iPS cell reprogramming. *Nature* **460**, 1136–1139 (2009).
10. Li, Y. *et al.* The p53-PUMA axis suppresses iPSC generation. *Nat Commun.* **4**, 2174 (2013).
11. Lake, B.B. *et al.* Context-dependent enhancement of induced pluripotent stem cell reprogramming by silencing Puma. *Stem Cells* **30**, 888–897 (2012).
12. Guo, S. *et al.* Nonstochastic reprogramming from a privileged somatic cell state. *Cell* **156**, 649–662 (2014).
13. Lee, Y.L. *et al.* Sirtuin 1 facilitates generation of induced pluripotent stem cells from mouse embryonic fibroblasts through the miR-34a and p53 pathways. *PLoS ONE* **7**, e45633 (2012).
14. Brosh, R. *et al.* p53 counteracts reprogramming by inhibiting mesenchymal-to-epithelial transition. *Cell Death Differ.* **20**, 312–320 (2013).
15. Ye, D. *et al.* MiR-138 promotes induced pluripotent stem cell generation through the regulation of the p53 signaling. *Stem Cells* **30**, 1645–1654 (2012).
16. Wang, J. *et al.* p53-facilitated miR-199a-3p regulates somatic cell reprogramming. *Stem Cells* **30**, 1405–1413 (2012).
17. Zhu, S. *et al.* Reprogramming of human primary somatic cells by OCT4 and chemical compounds. *Cell Stem Cell* **7**, 651–655 (2010).
18. Silva, J. *et al.* Promotion of reprogramming to ground state pluripotency by signal inhibition. *PLoS Biol.* **6**, e253 (2008).
19. Ichida, J.K. *et al.* A small-molecule inhibitor of Tgf-β signaling replaces *Sox2* in reprogramming by inducing *Nanog*. *Cell Stem Cell* **5**, 491–503 (2009).
20. Hou, P. *et al.* Pluripotent stem cells induced from mouse somatic cells by small-molecule compounds. *Science* **341**, 651–654 (2013).
21. Huangfu, D. *et al.* Induction of pluripotent stem cells by defined factors is greatly improved by small-molecule compounds. *Nat. Biotechnol.* **26**, 795–797 (2008).
22. Federation, A.J., Bradner, J.E. & Meissner, A. The use of small molecules in somatic-cell reprogramming. *Trends Cell Biol.* **24**, 179–187 (2014).
23. Amabile, G. & Meissner, A. Induced pluripotent stem cells: current progress and potential for regenerative medicine. *Trends Mol. Med.* **15**, 59–68 (2009).
24. Eminli, S. *et al.* Differentiation stage determines potential of hematopoietic cells for reprogramming into induced pluripotent stem cells. *Nat. Genet.* **41**, 968–976 (2009).
25. Gurdon, J.B. The developmental capacity of nuclei taken from intestinal epithelium cells of feeding tadpoles. *J. Embryol. Exp. Morphol.* **10**, 622–640 (1962).
26. Li, J., Greco, V., Guasch, G., Fuchs, E. & Mombaerts, P. Mice cloned from skin cells. *Proc. Natl. Acad. Sci. USA* **104**, 2738–2743 (2007).
27. Artavanis-Tsakonas, S. & Muskavitch, M.A. Notch: the past, the present, and the future. *Curr. Top. Dev. Biol.* **92**, 1–29 (2010).
28. Bray, S.J. Notch signalling: a simple pathway becomes complex. *Nat. Rev. Mol. Cell Biol.* **7**, 678–689 (2006).
29. Topley, G.I., Okuyama, R., Gonzales, J.G., Conti, C. & Dotto, G.P. $p21^{WAF1/Cip1}$ functions as a suppressor of malignant skin tumor formation and a determinant of keratinocyte stem-cell potential. *Proc. Natl. Acad. Sci. USA* **96**, 9089–9094 (1999).
30. Missero, C., Di Cunto, F., Kiyokawa, H., Koff, A. & Dotto, G.P. The absence of $p21^{Cip1/WAF1}$ alters keratinocyte growth and differentiation and promotes ras-tumor progression. *Genes Dev.* **10**, 3065–3075 (1996).
31. Aasen, T. & Belmonte, J.C. Isolation and cultivation of human keratinocytes from skin or plucked hair for the generation of induced pluripotent stem cells. *Nat. Protoc.* **5**, 371–382 (2010).
32. Aasen, T. *et al.* Efficient and rapid generation of induced pluripotent stem cells from human keratinocytes. *Nat. Biotechnol.* **26**, 1276–1284 (2008).
33. Blanpain, C., Lowry, W.E., Pasolli, H.A. & Fuchs, E. Canonical notch signaling functions as a commitment switch in the epidermal lineage. *Genes Dev.* **20**, 3022–3035 (2006).
34. Bock, C. *et al.* Reference maps of human ES and iPS cell variation enable high-throughput characterization of pluripotent cell lines. *Cell* **144**, 439–452 (2011).
35. Fuwa, H. *et al.* Divergent synthesis of multifunctional molecular probes to elucidate the enzyme specificity of dipeptidic γ-secretase inhibitors. *ACS Chem. Biol.* **2**, 408–418 (2007).
36. Nam, Y., Sliz, P., Song, L., Aster, J.C. & Blacklow, S.C. Structural basis for cooperativity in recruitment of MAML coactivators to Notch transcription complexes. *Cell* **124**, 973–983 (2006).
37. Nam, Y., Weng, A.P., Aster, J.C. & Blacklow, S.C. Structural requirements for assembly of the CSL.Intracellular Notch1.Mastermind-like 1 transcriptional activation complex. *J. Biol. Chem.* **278**, 21232–21239 (2003).
38. Lefort, K. & Dotto, G.P. Notch signaling in the integrated control of keratinocyte growth/differentiation and tumor suppression. *Semin. Cancer Biol.* **14**, 374–386 (2004).
39. Jones, P.H. & Watt, F.M. Separation of human epidermal stem cells from transit amplifying cells on the basis of differences in integrin function and expression. *Cell* **73**, 713–724 (1993).
40. Kavian, N. *et al.* Targeting ADAM-17/notch signaling abrogates the development of systemic sclerosis in a murine model. *Arthritis Rheum.* **62**, 3477–3487 (2010).
41. Allen, A.S. *et al.* *De novo* mutations in epileptic encephalopathies. *Nature* **501**, 217–221 (2013).
42. Huangfu, D. *et al.* Induction of pluripotent stem cells from primary human fibroblasts with only Oct4 and Sox2. *Nat. Biotechnol.* **26**, 1269–1275 (2008).
43. Mikkelsen, T.S. *et al.* Dissecting direct reprogramming through integrative genomic analysis. *Nature* **454**, 49–55 (2008).
44. Onder, T.T. *et al.* Chromatin-modifying enzymes as modulators of reprogramming. *Nature* **483**, 598–602 (2012).
45. Gore, A. *et al.* Somatic coding mutations in human induced pluripotent stem cells. *Nature* **471**, 63–67 (2011).

Acknowledgments

The authors would like to thank E. Son for assistance with microarray data analysis, S. Sato for assistance with chimera experiments, E. Kiskinis for assistance with nanostring analysis and K. Koszka and M. Yamaki for assistance with teratoma experiments. The authors are grateful for the financial support that made this work possible. K.E. was supported by US National Institutes of Health (NIH)

R01 grant 5R01GM096067, NIH P01 grant 5P01GM099117 and the Howard Hughes Medical Institute. A.M. was supported by NIH P01 grant 5P01GM099117. H.A. was supported by grants from the Ministry of Education, Culture, Sports, Science and Technology (MEXT) of Japan, Grant-in-aid for Scientific Research (21390456) and Grant-in-Aid for challenging Exploratory Research (22659304) and a grant from JST-CREST. J.K.I. was supported by a Stan and Fiona Druckenmiller–New York Stem Cell Foundation postdoctoral fellowship, NIH K99 grant 1K99NS077435-01A1, NIH R00 grant 4R00NS077435-03 and the Novartis Institutes for BioMedical Research. C.B. was supported by a Feodor Lynen Fellowship from the Alexander von Humboldt Foundation.

Author contributions

A.M. and J.E.B. hypothesized that Notch inhibition might aid reprogramming. J.K.I., J.T., A.M., A.U., L.L.R. and K.E. designed reprogramming and mechanistic experiments to test the hypothesis. J.K.I., J.T., A.C.C., L.A.W., Y.S., M.T.M., S.S., G.A. and H.A. performed reprogramming experiments and characterization of the iPSCs. C.B. and M.Z. performed bioinformatic analysis of transcriptional data characterizing the iPSCs. J.K.I., J.T., A.C.C. and Y.S. performed experiments to determine the mechanism of action of DAPT and Notch inhibition in reprogramming. K.E., J.K.I. and J.T. discovered and confirmed the mechanism of action of DAPT. K.E. and J.K.I. wrote the paper. All authors helped in paper revision.

Competing financial interests

The authors declare no competing financial interests.

Additional information

Supplementary information is available in the online version of the paper. Reprints and permissions information is available online at http://www.nature.com/reprints/index.html. Correspondence and requests for materials should be addressed to H.A., A.M. or K.E.

ONLINE METHODS

iPSC reprogramming experiments. The IACUC committee of Harvard University approved the use of mice for all experiments included in this paper. *Oct4*:GFP neonatal mouse keratinocytes were isolated from P1-P2 pups using an overnight digestion in either 0.25% trypsin/EDTA or TrypLE (Life Technologies) at 4 °C. They were cultured in SFM medium (Life Technologies) on collagen IV–coated plates. Neonatal human epidermal keratinocytes (Lonza) were cultured in Epilife medium (Invitrogen) on collagen-coated plates. Keratinocytes were reprogrammed using retroviruses containing either mouse or human *OCT4*, *SOX2*, *KLF4* and *CMYC* produced in the pMXs backbone. Chemical treatment was initiated 1–2 d after viral transduction and readministered every other day until the end of the experiment unless otherwise specified. DAPT (EMD Millipore) was used at 10 μM for reprogramming experiments using *OCT4*, *SOX2*, *KLF4* and *CMYC* and 2.5 μM for *OCT4*, *SOX2* reprogramming experiments unless otherwise noted. DBZ was used at 2 μM. Irradiated mouse embryonic fibroblast feeders were added 6 d after transduction, and the medium was changed to mouse or human embryonic stem cell medium at that time. Colonies were scored as iPSC colonies if they were *Oct4*::GFP+ in mouse experiments or NANOG+/TRA-1-81+ in human experiments.

Gene expression analysis of iPSCs. Nanostring (Nanostring Technologies) and scorecard analysis was performed as described[34]. iPSCs were cultured in mTesr1 medium (Stem Cell Technologies) before RNA isolation. To measure their differentiation propensities, iPSCs were dissociated into embryoid bodies and cultured in human embryonic stem cell medium without bFGF for 16 d. Cells were then lysed, and total RNA was extracted using Trizol (Life Technologies) and purified using the RNeasy kit (QIAGEN). 300–500 ng of RNA was profiled on the Nano-String nCounter system (Nanostring Technologies) according to the manufacturer's instructions. A custom nCounter codeset covering 500 genes that monitor cell state, pluripotency and differentiation was used[34]. Data analysis was performed with the R statistics package as in ref. 34. Briefly, the lineage scorecard performs a parametric gene set enrichment analysis on *t* scores obtained from a pairwise comparison between the cell line of interest and the reference of ES cell–derived EBs.

Differentiation of iPSCs. For teratoma formation, 1–2 million human iPSCs were injected into the kidney capsule of nude mice and harvested 2 months later. Teratomas were sectioned and stained with hematoxylin and eosin for visualization. For the mouse iPSC chimera assay, 10 *Oct4*::GFP+ iPSCs were injected per ICR blastocyst, and 20 blastocysts were transplanted into each pseudopregnant female. Embryos were either allowed to develop to term or harvested at day E12.5 and dissected for genital ridge analysis using a stereomicroscope.

Gene expression analysis of reprogramming cultures. Illumina MouseRef-8 microarrays (Illumina) were used for genome-wide mRNA expression analysis of reprogramming mouse keratinocyte cultures treated with DMSO or 10 μM DAPT. For qPCR analysis, RNA was isolated using Trizol, cDNA synthesis was performed using the iScript cDNA synthesis kit (Bio-Rad), and the SYBR Green qPCR Supermix (Bio-Rad) was used for PCR product detection.

Western blots and immunofluorescence. Antibodies detecting mouse Notch (Santa Cruz Biotechnology, sc-6015, 1:1,000), human NOTCH (Abcam, ab27526, 1:1,000 and Santa Cruz Biotechnology, sc-23307, 1:1,000), cleaved human NOTCH (Cell Signaling Technology, 2421, 1:1,000), p53 (Santa Cruz Biotechnology, sc-56182, 1:1,000), Involucrin (Abcam, Ab53112) and p21 (Cell Signaling Technology 05-345, 1:1,000) were used for western blots. Blots were quantified using ImageJ software. Antibodies specific for NANOG (Abcam, AF1997, 1:400) and TRA-1-81 (Chemicon, MAB4381, 1:500) were used to identify human iPSCs. A γH2AX (Abcam, ab11175, 1:400) antibody was used to detect γH2AX foci. Cells in which γH2AX staining covered greater than half the nucleus were scored as positive for γH2AX foci.

UV irradiation assay. UV irradiation was performed at a dosage of 30 J. TUNEL staining was performed using a TUNEL kit (Pharmacia Biosciences).

shRNA and siRNA knockdown experiments. shRNAs and siRNAs were purchased from Sigma and added to reprogramming cultures within 1 d after addition of the reprogramming retroviruses. shRNAs (TRCN0000003753, p53 and TRCN0000287021, p21) were expressed in the pLKO.1 lentiviral backbone. siRNAs were used at 80 nM and were transfected into reprogramming cultures using RNAiMAX (Life Technologies).

Array CGH analysis of iPSC lines. Cell Line Genetics performed array CGH analysis of iPSC lines at passage 5 using 4x180K+SNP analysis.

Statistical analysis. For all experiments, error bars represent the s.d. between two or three biological replicates, and statistical significance was determined using a two-tailed homoscedastic Student's *t*-test.

doi:10.1038/nchembio.1552

ERRATUM

Notch inhibition allows oncogene independent generation of iPS cells

Justin K Ichida, Julia T C W, Luis A Williams, Ava C Carter, Yingxiao Shi, Marcelo T Moura, Michael Ziller, Sean Singh, Giovanni Amabile, Christoph Bock, Akihiro Umezawa, Lee L Rubin, James E Bradner, Hidenori Akutsu, Alexander Meissner & Kevin Eggan

Nat. Chem. Biol. **10**, 632–639 (2014); published online 22 June 2014; corrected after print 29 July 2014.

In the version of this article initially published, Julia TCW's name was misspelled as Julia T C W. In addition, her initials in the author contribution statement should have read J.T. instead of J.T.C.W. The error has been corrected in the HTML and PDF versions of the article.

ERRATUM

Notch inhibition allows oncogene-independent generation of iPS cells.

Justin K Ichida, Julia T C W, Luis A Williams, Ava C Carter, Yingxiao Shi, Marcelo T Moura, Michael Ziller, Sean Singh, Giovanni Amabile, Christoph Bock, Akihiro Umezawa, Lee L Rubin, James E Bradner, Hidenori Akutsu, Alexander Meissner & Kevin Eggan

Nat. Chem. Biol. **10**, 632–639 (2014); published online 22 June 2014; corrected after print 29 July 2014 and 14 August 2014

In the version of this article initially published, a black bar was erroneously placed in the scrambled shRNA column in Figure 3g. The error has been corrected for the PDF and HTML versions of the article.

ARTICLE
PUBLISHED ONLINE: 22 JUNE 2014 | DOI: 10.1038/NCHEMBIO.1552
nature chemical biology

Notch inhibition allows oncogene-independent generation of iPS cells

Justin K Ichida[1,2,9,10], Julia TCW[1-3,10], Luis A Williams[1,2], Ava C Carter[1,2], Yingxiao Shi[9], Marcelo T Moura[1,2], Michael Ziller[1,4], Sean Singh[1,2], Giovanni Amabile[5], Christoph Bock[1,4], Akihiro Umezawa[6], Lee L Rubin[1], James E Bradner[7,8], Hidenori Akutsu[6]*, Alexander Meissner[1,4]* & Kevin Eggan[1-3]*

The reprogramming of somatic cells to pluripotency using defined transcription factors holds great promise for biomedicine. However, human reprogramming remains inefficient and relies either on the use of the potentially dangerous oncogenes *KLF4* and *CMYC* or the genetic inhibition of the tumor suppressor gene *p53*. We hypothesized that inhibition of signal transduction pathways that promote differentiation of the target somatic cells during development might relieve the requirement for non-core pluripotency factors during induced pluripotent stem cell (iPSC) reprogramming. Here, we show that inhibition of Notch greatly improves the efficiency of iPSC generation from mouse and human keratinocytes by suppressing p21 in a p53-independent manner and thereby enriching for undifferentiated cells capable of long-term self-renewal. Pharmacological inhibition of Notch enabled routine production of human iPSCs without KLF4 and CMYC while leaving p53 activity intact. Thus, restricting the development of somatic cells by altering intercellular communication enables the production of safer human iPSCs.

Use of the potent oncogenes *KLF4* and *MYC* (henceforth referred to as *CMYC*) in the generation of iPSCs limits their translational utility[1,2]. Currently, elimination of these genes during human iPSC reprogramming requires suppression of p53 activity[2–16], which in turn results in the accumulation of genetic mutations in the resulting iPSCs[8]. Therefore, there remains a real need for reprogramming approaches that enable iPSC generation without the use of *KLF4* and *CMYC* while leaving p53 activity intact.

In part to address this need, several groups have undertaken chemical screens to identify small molecules that can improve reprogramming[17–21]. Thus far, the majority of active compounds are thought to improve reprogramming by inhibiting chromatin-modifying enzymes or by reinforcing the transcriptional network associated with the pluripotent state[17–22]. Consistent with their proposed mechanisms of action, these chemicals generally function in cellular intermediates that arise late in reprogramming, catalyzing their final conversion into iPSCs[19,22]. It is currently unclear whether known chemicals are sufficient for generating iPSCs from adult human cells, which are consistently more difficult to reprogram than mouse embryonic fibroblasts[23].

Given the likely need for additional reprogramming chemicals and the knowledge that most known compounds act late in this process, we reasoned that it would be valuable to identify small molecules that improve reprogramming by acting early, perhaps within the somatic cells themselves. We reasoned that one approach toward this goal would be to identify chemicals that could modulate signal transduction cascades in somatic cell populations to enrich for those cells with an enhanced capacity for reprogramming. We reasoned that if such compounds could be identified, they might expand the translational utility of chemical reprogramming.

It has been recognized that the extent of a target cell's differentiation is an important determinant of the efficiency by which it can be reprogrammed[24–26]. We therefore hypothesized that chemically driving somatic cells into a more potent 'stem cell' state might improve their reprogramming. To test this hypothesis, we chose to ask whether known chemical inhibitors of the Notch signaling pathway could aid in reprogramming.

The Notch signaling pathway is highly conserved and regulates the proliferation and differentiation of many distinct progenitor cell and stem cell types[27]. Notch ligands are generally transmembrane proteins that require contact between two cells to mediate signal transduction[28]. In skin, Notch promotes differentiation by directly activating *CDKN1A* (henceforth referred to as *p21*) expression, which in turn blocks proliferation and induces the differentiation of keratinocyte stem cell populations[29,30]. We therefore hypothesized that inhibition of Notch in keratinocytes might enhance iPSC generation by inhibiting differentiation and enriching more easily reprogrammed progenitor cells. We also felt that keratinocytes were an attractive model for testing our hypothesis because if Notch inhibition did have an effect, it could be immediately translated to the production of patient-specific iPSCs[31,32].

Here, we show that Notch inhibition improves the efficiency of iPSC generation from mouse and human keratinocytes by suppressing p21 and thereby enriching undifferentiated cells with increased reprogramming potential. In addition, pharmacological inhibition of Notch enabled the efficient production of human iPSCs without *KLF4* and *CMYC* while leaving p53 activity intact, resulting in the production of safer human iPSCs.

[1]Harvard Stem Cell Institute, Department of Stem Cell and Regenerative Biology, Harvard University, Cambridge, Massachusetts, USA. [2]Howard Hughes Medical Institute, Stanley Center for Psychiatric Research, Cambridge, Massachusetts, USA. [3]Department of Molecular and Cellular Biology, Harvard University, Cambridge, Massachusetts, USA. [4]Broad Institute of MIT and Harvard, Cambridge, Massachusetts, USA. [5]Harvard Stem Cell Institute, Harvard Medical School, Boston, Massachusetts, USA. [6]Department of Reproductive Biology, National Research Institute for Child Health and Development, Tokyo, Japan. [7]Department of Medical Oncology, Dana-Farber Cancer Institute, Boston, Massachusetts, USA. [8]Department of Medicine, Harvard Medical School, Boston, Massachusetts, USA. [9]Department of Stem Cell Biology and Regenerative Medicine, University of Southern California, Los Angeles, California, USA. [10]These authors contributed equally to this work. *e-mail: akutsu-h@ncchd.go.go.jp, alexander_meissner@harvard.edu or keggan@scrb.harvard.edu

RESULTS

DAPT treatment promotes keratinocyte reprogramming

Notch signaling is activated by the γ-secretase complex, which cleaves the membrane-tethered Notch receptor upon ligand binding and generates a free intracellular domain that can translocate to the nucleus and modulate transcription[27]. It has previously been shown that the γ-secretase inhibitor DAPT (**Fig. 1a**) can block Notch signaling in mouse keratinocytes[33]. As expected, 10 μM DAPT treatment of both neonatal mouse and human keratinocytes transduced with the iPSC reprogramming factors increased the abundance of the full-length Notch receptor, reduced levels of cleaved Notch intracellular domain (**Supplementary Results**, **Supplementary Fig. 1a**) and decreased expression of the Notch-target genes *Hey1*, *Hes1*, *Hes5* and *Col6a1* (**Supplementary Fig. 1b**).

To determine whether inhibition of Notch could increase the efficiency of reprogramming, we used *Pou5f1* (henceforth referred to as *Oct4*), *Sox2*, *Klf4* and *cMyc* to transduce *Oct4*::GFP mouse or human keratinocytes and cultured the resulting cells for 25 d either in the presence or absence of DAPT. We found that the addition of 10 μM DAPT led to a fourfold increase in the number of resulting *Oct4*::GFP+ mouse and NANOG+/TRA-1-81+ human iPSC colonies (**Fig. 1b**).

We wondered whether this increase in reprogramming activity might allow the generation of iPSCs from keratinocytes without *Klf4* and *cMyc*. Indeed, although transduction of *Oct4* and *Sox2* alone were not sufficient to induce keratinocyte reprogramming, *Oct4* and *Sox2* combined with DAPT treatment routinely yielded mouse and human iPSC colonies (**Fig. 1c,d** and **Supplementary Fig. 2a**). This effect was specific to *Oct4*- and *Sox2*-transduced cells because other two-factor combinations did not yield iPSCs in the presence of DAPT (**Fig. 1c**).

To determine whether these putative iPS cell lines were pluripotent, we subjected them to a 'scorecard' assay for pluripotency that we recently developed[34]. We found that these cell lines were indeed composed of pluripotent cells and that they performed comparably to human embryonic stem cells in their expression of pluripotency-associated genes and differentiation propensities (**Supplementary Fig. 2b,c**). To further confirm their differentiation capacity, we also injected the *OCT4*, *SOX2*+ DAPT human cells into immunocompromised mice and found that they readily formed teratomas containing differentiated cells (**Fig. 1e**). Moreover, when injected into blastocysts, the *Oct4*, *Sox2*+ DAPT mouse cells contributed to the germline, producing chimeric mice (**Supplementary Fig. 2d,e**).

Many applications of iPSCs would require the DAPT-dependent generation of *KLF4*- and *CMYC*-free iPSCs from adult keratinocytes. Therefore, we determined whether DAPT treatment increased the reprogramming potential of adult human keratinocytes. As with mouse and human neonatal keratinocytes, we found that DAPT treatment of *KLF4*-, *SOX2*-, *OCT4*- and *CMYC*-transduced adult human keratinocytes markedly improved their rate of reprogramming (**Supplementary Fig. 2f**) and also enabled the generation of iPSCs with just *OCT4* and *SOX2* (**Fig. 1f** and **Supplementary Fig. 2g**). The scorecard assay again verified that these two-factor iPSCs were pluripotent (**Supplementary Fig. 2b,c**). Together, these results demonstrate that DAPT reliably enables the generation of bona fide mouse and human iPSCs from keratinocytes without *KLF4* and *CMYC*.

Notch inhibition promotes reprogramming

Our results thus far suggest that antagonizing Notch signaling in keratinocytes may promote their conversion into iPSCs. To begin verifying that NOTCH was indeed the functional target of DAPT during reprogramming, we tested a structurally distinct γ-secretase inhibitor, DBZ[35] (**Fig. 2a**), for activity in iPSC generation. When we treated human keratinocytes with DBZ, we observed

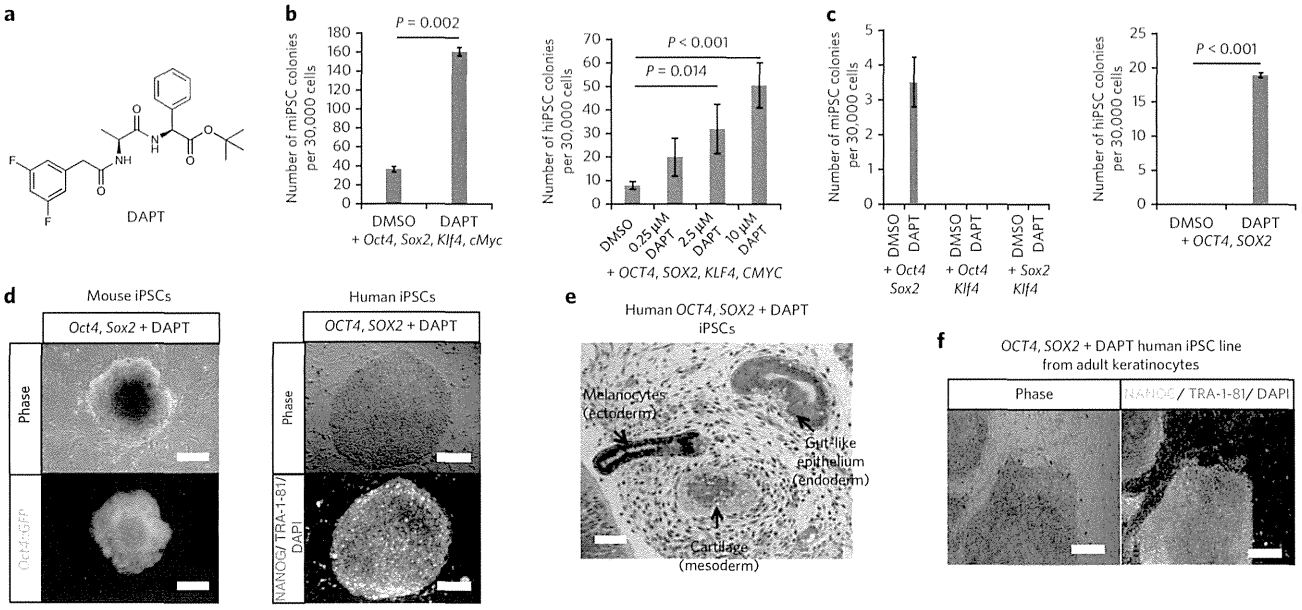

Figure 1 | DAPT treatment promotes mouse and human keratinocyte reprogramming. (**a**) Chemical structure of DAPT. (**b**) The efficiency of iPSC generation from mouse (left) and human (right) keratinocytes transduced with *Oct4*, *Sox2*, *Klf4* and *cMyc* with DMSO or DAPT treatment (DAPT used at 10 μM in mouse experiment). (**c**) The efficiency of iPSC generation from mouse (left) and human (right) keratinocytes transduced with all combinations of two reprogramming factors with DMSO or 2.5 μM DAPT treatment from days 1–18 after transduction. (**d**) A P0 mouse and human iPSC colony generated using *OCT4*, *SOX2* and DAPT. Scale bars, 100 μm. (**e**) Teratoma generated by iPSCs derived from human neonatal kerationcytes using *OCT4*, *SOX2* and DAPT. Scale bar, 50 μm. (**f**) NANOG+/TRA-1-81+ iPSC line generated from human adult keratinocytes using *OCT4*, *SOX2*+ DAPT. Scale bars, 100 μm. For all experiments, error bars represent the s.d. between two or three biological replicates, and statistical significance was determined using a two-tailed homoscedastic Student's *t*-test.